Available online at www.sciencedirect.com
SCIENCE DIRECT®
Journal of Nuclear Materials 335 (2004) 121–145
journal of nuclear materials
www.elsevier.com/locate/jnucmat

Simulation of radiation damage in Fe alloys: an object kinetic Monte Carlo approach

C. Domain [a], C.S. Becquart [b,*], L. Malerba [c]

[a] Electricité de France, EDF – R&D, Dpt Matériaux et Mécanique des Composants, Les Renardières, F-77250 Moret sur Loing, France
[b] Laboratoire de Métallurgie Physique et Génie des Matériaux, UMR 8517, Bât. C6, Université Lille I, F-59655 Villeneuve d'Ascq cédex, France
[c] SCK•CEN (Belgian Nuclear Research Centre), Department Materials Reactor Research – Boeretang 200, B-2400 Mol, Belgium

Received 6 October 2003; accepted 12 July 2004

Abstract

The reactor pressure vessel (RPV) steels used in current nuclear power plants embrittle as a consequence of the continuous irradiation with neutrons. Among other radiation effects, the experimentally observed formation of copper-rich defects is accepted to be one of the main causes of embrittlement. Therefore, an accurate description of the nucleation and growth under irradiation of these and other defects is fundamental for the prediction of the mechanical degradation that these materials undergo during operation, with a view to guarantee a safer plant life management. In this work we describe in detail the object kinetic Monte Carlo (OKMC) method that we developed, showing that it is well suited to investigate the evolution of radiation damage in simple Fe alloys (Fe, Fe–Cu) under irradiation conditions (temperature, dose and dose-rate) typical of experiments with different impinging particles and also operating conditions. The still open issue concerning the method is the determination of the mechanisms and parameters that should be introduced in the model in order to correctly reproduce the experimentally observed trends. The state-of-the-art, based on the input from atomistic simulation techniques, such as ab initio calculations, molecular dynamics (MD) and atomic kinetic Monte Carlo, is critically revised in detail and a sensitivity study on the effects of the choice of the reaction radii and the description of defect mobility is conducted. A few preliminary, but promising, results of favorable comparison with experimental observations are shown and possible further refinements of the model are briefly discussed.
© 2004 Elsevier B.V. All rights reserved.

1. Introduction

Low alloy ferritic steels are structural materials for the pressure vessels of light water reactors and are long known to undergo severe embrittlement under neutron irradiation during operation [1–5]. The microscopic mechanisms responsible for this effect are nowadays qualitatively fairly well understood in terms of matrix damage accumulation, radiation-enhanced copper precipitation and, to a lesser extent, grain boundary segregation [2,3]. However, these nanofeatures are mostly below the resolution of the electron microscope and only the combination of advanced experimental techniques has recently enabled to better characterise their nature

* Corresponding author. Tel.: +33 320 436927; fax: +33 320 434040.
E-mail address: charlotte.becquart@univ-lille1.fr (C.S. Becquart).

0022-3115/$ - see front matter © 2004 Elsevier B.V. All rights reserved.
doi:10.1016/j.jnucmat.2004.07.037

[3], while a number of significant uncertainties remain. Copper-rich precipitates are known to appear in the form of a relatively high density of ultrafine (<2 nm) particles, whose composition (Ni, Mn and particularly Fe content) and morphology (clouds or full precipitates) is still being debated [4–6]. The matrix damage component is generally interpreted as a collection of point defect clusters, such as self-interstitial atom (SIA) loops and nanovoids, although their exact nature, in combination and interaction with solute atoms, remains elusive [3]. The kinetics of nucleation and growth of all these features, as well as their stability, which are the basic ingredients for the elaboration of physically-grounded predictive models for hardening and embrittlement, are far from being well known. However, the difficulty of exploring experimentally the involved nanoscales can be nowadays relieved with the more and more widespread use of adequate numerical simulation tools.

It is now clearly established that neutron interaction with matter leads to the formation of displacement cascades, thereby producing the so-called primary damage: small regions containing a core of vacancies, either isolated or grouped in small clusters, surrounded by SIA, themselves either isolated or in clusters [7–9]. The formation of these primary defects in displacement cascades is too fast, and their size generally too small, to be observed experimentally, but molecular dynamics (MD) simulations have proven to be a powerful tool to study displacement cascades, as well as the morphology of the produced defects, their mutual interaction and, to some extent, also their evolution [9–20]. However, because of the short timespan covered by MD simulations (10–15 ps for volumes large enough to contain a displacement cascade, i.e. of the order of tens of nanometers), other computational tools must be used to extend the study up to the formation of experimentally resolvable damage features.

This paper presents the kinetic Monte Carlo (KMC) approach we use to study the long term evolution of vacancies and SIA left by the accumulation of displacement cascades in Fe and Fe–Cu [19,20], as model systems for RPV steels, including the interaction of point defects with solute atoms (Cu), traps and sinks. The purpose of the paper is to discuss critically and in detail assumptions that have been widely used in the recent past by different authors, in order to identify a KMC parameter set capable of reproducing radiation damage evolution in Fe alloys, in an acceptable trade-off between reliability and computing time, within the simplified framework that corresponds to the state-of-the-art [21–25]. This, as will be discussed, will be the basis for further refinements of the model.

Two complementary kinetic Monte Carlo (KMC) methods have been developed, both of them part of the LAKIMOCA package [26,27]. The first one, referred to as Atomistic KMC (AKMC), reproduces in detail the diffusion of vacancies and solute atoms via first neighbour jumps in an iron matrix, thereby leading to the formation of voids and precipitates, but cannot describe other defects, such as SIA and SIA clusters. This model has been already described and applied in previous work [26–28]. The second one, denoted as 'object' KMC (OKMC), can treat all point defects (vacancies and SIA), point defect clusters (e.g. nanovoids and dislocation loops) and mixed clusters containing also solute atoms (copper-vacancy complexes) as 'objects', each of them characterised by type, size, shape, position in the simulation box and volume of interaction, as well as by a series of possible actions (migration, emission) and reactions with other objects (formation of larger clusters, interaction with solute atoms and traps randomly distributed in the simulation volume, annihilation at sinks, etc.). The model can describe the fate of the objects included in it up to times on the order of the lifetime of a reactor vessel (30–40 years), both in simple cases (evolution of a single cascade, or 'cascade ageing') and reproducing electron, ion or neutron irradiation conditions, at realistic dose rates (from 10^{-4} down to 10^{-11} dpa/s), up to significant doses (0.1–1 dpa), within a reasonable amount of computing time (few days at the most), in simulation volumes up to 10^6 nm^3 ($\sim$100 nm typical length). The actual performance of the code to simulate different conditions, in terms of computing time, is reported in Appendix A to this paper. To our knowledge, similar OKMC approaches have been hitherto used extensively to study radiation damage in pure elements [21–25], but hardly any attempt has been made to treat alloys, except in a different KMC approach, which treats reactions between defects in term of events [29] and, very recently, by explicitly introducing the effects of He in Fe [30].

In Section 2 the main assumptions of our model are explained and discussed in detail and three different possible choices of parameters are proposed, based on the input from atomistic simulations (ab initio calculations, MD and AKMC results), as well as from OKMC and rate theory (RT) models available from the literature and, when available, experimental observations. Section 3, where the results of the application of the model are presented, is divided into two parts. In the first one, the results of a parameter sensitivity study on cascade ageing simulations are reported. The importance of the statistical treatment of the data for this type of studies is stressed and the choice of parameters such as point-defect migration energies and capture radii is discussed. In the second part the model is used to reproduce irradiation experiments taken from the literature, performed with different impinging particles and in different irradiation conditions. This application allows us to propose a basic set of parameters that, within the limits of the assumptions made in Section 2, is capable of describing acceptably the behaviour of Fe

and Fe–Cu alloys under irradiation. Finally, a brief discussion of limitations and possible improvements of the current models is given.

2. Computational procedure

2.1. Main assumptions of the model

The objects treated in the OKMC model have defined centre-of-mass positions in space, corresponding to *bcc* lattice sites, and (when they are supposed to) they migrate according to lattice distances, but no real *atomic* lattice exists in the model. They can be point-defects and point-defect clusters, interacting with solute atoms to form mixed complexes, as well as with generic traps, that can be broadly assumed to simulate the effect of interstitial impurities but in fact include also other effects (see Section 4).

At the moment, two possible shapes can be associated to point defect clusters: spherical (e.g. 3D nanovoids) or 2D platelets (e.g. SIA loops). The choice of the shape is a free parameter: in the case of Fe, for instance, vacancy clusters and mixed solute-vacancy complexes are always assumed to be spherical, while SIA clusters above a certain size can be assumed to be loops. In this work all clusters have been defined as spherical, to follow the assumptions commonly used in OKMC models [21–25]. In the discussion section possible improvements to this rough assumption are addressed.

Time elapses according to a residence time algorithm [31], as described below. During the simulation, internal and external events can occur, whose probabilities of occurrence are expressed in terms of frequencies (in s^{-1}). According to the basic MC algorithm, among all the possible events, one and only one is chosen at each timestep, by extracting a random number between 0 and 1 and multiplying it times the sum of all probabilities.

2.1.1. Internal events

The objects can experience five types of internal events:

- Jump to a neighbouring site.
- Recombination with objects of opposite type (i.e. SIA with vacancies) or aggregation with other objects (e.g. point-defect clusters and complexes including solute atoms).
- Dissociation (when the object is big enough and dissociation is allowed) by emission of one element (e.g. single-vacancy) from the object.
- Trapping or annihilation at free surfaces, grain boundaries, dislocations or other sinks.

Table 1 summarises the different internal events which can take place in the simulations for pure Fe and Fe–Cu alloys. No direct interactions between solute atoms and SIA is considered in this work, as will be explained later.

Table 1
Possible object reactions in the case of Fe–Cu alloys: S stands for solute, V for vacancy, I for SIA, T for traps and FS for free surfaces (or sinks)

Events	Reactions for pure elements	Reactions with solute atoms
SIA aggregation	$m\mathrm{I} + m'\mathrm{I} \rightarrow (m+m')\mathrm{I}$	–
V aggregation	$m\mathrm{V} + m'\mathrm{V} \rightarrow (m+m')\mathrm{V}$	$[m\mathrm{V} + n\mathrm{S}] + [m'\mathrm{V} + n'\mathrm{S}] \rightarrow [(m+m')\mathrm{V} + (n+n')\mathrm{S}]$
SIA emission	$(m+1)\mathrm{I} \rightarrow \mathrm{I} + m\mathrm{I}$	–
V emission	$(m+1)\mathrm{V} \rightarrow \mathrm{V} + m\mathrm{V}$	$[(m+1)\mathrm{V} + n\mathrm{S}] \rightarrow [m\mathrm{V} + n\mathrm{S}] + \mathrm{V}$ $[(m+1)\mathrm{V} + (n+1)\mathrm{S}] \rightarrow [m\mathrm{V} + n\mathrm{S}] + [\mathrm{V} + \mathrm{S}]$
Recombination	$n\mathrm{I} + m\mathrm{V} \rightarrow \begin{cases} (n-m)\mathrm{I} & (\text{if } n > m) \\ (m-n)\mathrm{V} & (\text{if } m > n) \\ \varnothing & (\text{if } m = n) \end{cases}$	$n\mathrm{I} + [m\mathrm{V} + p\mathrm{S}] \rightarrow \begin{cases} (n-m)\mathrm{I} + p\mathrm{S} & (\text{if } n > m) \\ [(m-n)\mathrm{V} + p\mathrm{S}] & (\text{if } m > n) \\ p\mathrm{S} & (\text{if } m = n) \end{cases}$
SIA trapping	$m\mathrm{I} + \mathrm{T} \leftrightarrow [m\mathrm{I} + \mathrm{T}]$	–
V trapping	$m\mathrm{V} + \mathrm{T} \leftrightarrow [m\mathrm{V} + \mathrm{T}]$	$[m\mathrm{V} + n\mathrm{S}] + \mathrm{T} \leftrightarrow [m\mathrm{V} + n\mathrm{S} + \mathrm{T}]$
Surface	$m\mathrm{I} + \mathrm{FS} \leftrightarrow \mathrm{FS}$	–
Surface	$m\mathrm{V} + \mathrm{FS} \leftrightarrow \mathrm{FS}$	$[m\mathrm{V} + n\mathrm{S}] + \mathrm{FS} \leftrightarrow n\mathrm{S} + \mathrm{FS}$

The size of the objects is denoted by the integer numbers m, m', n, n' and p. Brackets enclose mixed objects.

Jump and dissociation probabilities $\Gamma_{n,i}$ (for object n and event i) are considered as thermally activated processes, characterised by an activation energy $E_{a,n,i}$ and an attempt frequency $\nu_{n,i}$:

$$\Gamma_{n,i} = \nu_{n,i} \exp\left\{-\frac{E_{a,n,i}}{kT}\right\}. \quad (1)$$

For the object jump, the activation energy is its migration energy, E_m. For the emission from either a trap or an object, E_a equals $E_m + E_b$, where E_b is the binding energy of the escaping entity (e.g. that of a single vacancy or SIA from a cluster) and E_m its migration energy. Note that, in the case of complexes containing both vacancies and solute atoms, only the emission of either a single vacancy or a mixed vacancy-solute pair is considered. An alternative point of view, not used in this work, consists in the emission of single solute atoms. The theoretically possible emission of vacancies from large SIA loops is neglected. Note also that in a real diffusion event, on a real lattice, the emitted particle has to perform several jumps to escape the source object. In our model, the escaping object is therefore placed at a distance such that, at the following step, both recombination with the initial object and diffusion away are possible, thus $\Gamma_{n,i}$ is only an approximation of the escaping probability.

Trapping and annihilation of defects with opposite defects or at sinks, as well as aggregation into larger clusters, take place spontaneously whenever the involved objects come to a mutual distance smaller than a reaction distance, which is equal to the sum of the capture radii associated to each of the two objects, as explained in the description of the parameter sets. The capture radius depends on the object type, size and shape. Free surfaces, grain boundaries and dislocation lines (segments) are the sinks that can be currently introduced in the model. However, in the simulations presented in this work dislocations were not inserted. More details are given in Section 2.1.4.

2.1.2. External events

In the course of the simulations, different types of external events can take place, depending upon the kind of irradiation that is simulated. All external events are characterised by occurrence probabilities P_m (for event m), corresponding to the production rate:

$$P_m = (\text{number of external events/cm}^3/\text{s}) \times (\text{simulation box volume}). \quad (2)$$

The production rate is determined from the flux of impinging particles, as described in what follows.

2.1.2.1. Neutron and ion irradiation. The impinging neutron flux is transformed into a production rate (number per unit time and volume) of randomly distributed displacement cascades of different energies (5, 10, 20,... keV), as well as residual Frenkel pairs. This is done using a combination of a neutron transport code (SPECTER [32]) to estimate the primary knock-on atom (PKA) spectrum and an analytical transport method to assess the cascade splitting into smaller subcascades (INCAS code [33]). Accordingly, new cascade debris are injected randomly in the simulation box, at the corresponding rate. In order to introduce more variability, the system of co-ordinates to which the cascade debris was originally referred to is, each time, randomly permuted relative to the simulation box co-ordinates. The accumulated dpa are calculated using the NRT formula [34]:

$$\text{displacements per cascade} = \frac{0.8E_{MD}}{2E_D}, \quad (3)$$

where E_{MD} is the damage energy, i.e. the fraction of the kinetic energy of the PKA that is not absorbed by electronic excitation, equivalent to the energy by which the input cascade had been initiated in the MD simulation, and E_D is the displacement threshold energy (40 eV for Fe [35]).

This approach is equally used to simulate ion irradiation, using only cascade debris input, without a need for PKA spectrum calculation. The production rate is calculated directly from the impinging ion flux, assuming all ions to have rigorously the same energy. The production rate distribution along the range of ion penetration is also taken into account by using a PKA density distribution profile which can be obtained with codes such as TRIM. However, in the present work no simulations of ion irradiation will be reported.

2.1.2.2. Electron irradiation. In the case of an electron irradiation simulations, Frenkel pairs are introduced randomly in the simulation box according to a certain dose rate, assuming – as an acceptable first approximation – that each electron is responsible for the formation of only one Frenkel pair. The corresponding SIA and vacancy can have both correlated or non correlated positions: in the former case the distance between SIA and vacancy is below a critical value and they may undergo quick recombination; in the latter both are introduced randomly.

2.1.3. Timestep determination

At each timestep an event is chosen by extracting a random number that can be associated to one and only one possible internal or external event, according to its probability. The associated average timestep length is given by:

$$\Delta t = \frac{1}{\sum_{n,i}\Gamma_{n,i} + \sum_m P_m}, \quad (4)$$

where the summation is extended over all the possible internal and external events at the considered step. This approach corresponds to the residence time algorithm for lattice KMC methods [31]. Alternative approaches [36–38] have been observed to be equivalent, in practice, to Eq. (4).

2.1.4. Boundary conditions and sinks

The boundary conditions can be adapted to correspond to different possible real situations: uniformly distributed events in bulk materials, isolated events (like single displacement cascades) in an otherwise untouched infinite material and, for both possibilities, thin foils, like in electron microscope or ion irradiated specimens. In order to allow the comparison with the irradiation of atom-probe needle-shaped specimens, a cylindrical box can also be used, which reproduces the truncated part of the needle. Accordingly, the boundary conditions can be either periodic (PBC: any defect that leaves the box re-enters it from the opposite side), or absorbing (the defects leaving the box disappear for good). In the case of thin foil and atom-probe needle simulations, free surfaces are correspondingly introduced. Grain boundaries, which act as sinks for point defects in the absence of free surfaces, are introduced using the average grain size method, inspired by Heinisch's work [39]: when PBC are applied, whenever a mobile object has moved a distance larger than the average grain size, it is eliminated. Recently, this method has been discussed by Soneda et al. [25] and denoted as *finite* PBC. Dislocations are introduced as segment(s) whose length is established according to the dislocation density to be simulated. They act as linear sinks for point-defects with a given recombination radius. Fig. 1 summarizes the different events taking place in the course of an object KMC simulation.

2.2. Parameter sets

The choice of the parameter set is quite an open question and several possibilities have been proposed to simulate radiation damage by KMC in pure Fe [21–25]. The defects produced by irradiation in ferritic steels are very difficult to characterise experimentally, even using the most advanced techniques nowadays available, as they are very small, and remain small in the course of the irradiation. SIA loops are observed to form under electron, neutron and ion irradiation in pure Fe [40–42]. Recently, precise experiments of in situ electron irradiation of pure Fe thin foils were performed [43] and important information concerning the kinetics of growth of SIA dislocation loops in pure Fe is hence available to adjust the parameters of KMC simulations. Vacancy loops have been seen to form in Fe under heavy ion irradiation conditions [44], but do not seem to have ever been observed under neutron irradiation [45], particularly in conditions relevant to RPV steels in operation. Voids become visible only at high doses, never attained in pressure vessel steels [46], although their presence below electron microscope resolution is testified by positron annihilation studies [47–50]. In the case of Fe alloys, such as Fe–Cu, the situation is even more complicated because, in spite of a growing number of experimental studies of the behaviour of Fe–Cu under irradiation in different conditions [48,51–55], many pieces of information of fundamental importance for the simulation, such as those concerning the interaction strength of point-defects and point-defect clusters with solute atoms, cannot be obtained experimentally and its calculation requires to consider a large number of possible cases.

In the present study, three main first attempt sets of parameters have been used and compared. These parameter sets try to encompass the most common choices of OKMC and also RT models available from Refs. [21–23,43]. Parameter tuning made necessary to improve the performance of the model when trying to reproduce experimental results and possible refinement to the current framework are discussed in the course of the present paper.

The first one (set A) is inspired by experimental results by Hardouin Duparc et al. and a related rate theory

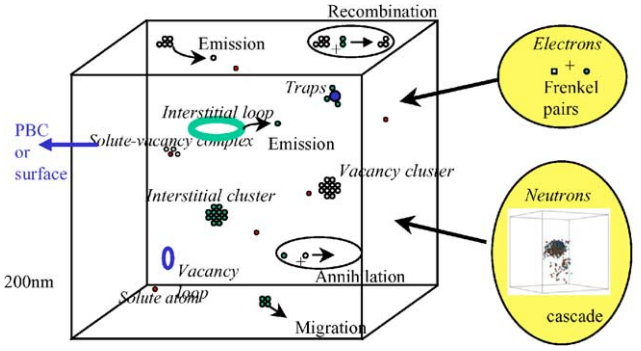

Fig. 1. Summary of the different events taking place in an object KMC simulation. Note that loops, characterised by non-spherical reaction volume, though allowed for in the code, have not been included in the model in the present work.

model [43]. In this model, defect mobilities and migration energies were adjusted to reproduce the loop number density observed by transmission electron microscopy (TEM). In the corresponding parameter set, only single point defects are allowed to move and the migration energies are tuned to effective values that include possible trapping effects at interstitial impurities (C,N). The second set of parameters (set B) is based on atomistic simulations results, which suggest that also vacancy and SIA clusters are mobile, with migration energies that are lower than the effective values used in set A [21,56–60]. This choice is consistent with previous KMC studies [21–25]. Finally, the third set (set C) is intermediate between the previous ones: the migration energies are those stemming from atomistic simulations (like in set B), but only single point defects are allowed to move (like in set A).

2.2.1. Capture radii

The notion of capture radius originates from the rate theory applied to radiation damage [61]. It is related to the distance at which point defects are absorbed in sinks and, more broadly, at which different defects interact with each other. For a cluster of type α (either SIA, $\alpha = \mathrm{I}$, or vacancies, $\alpha = \mathrm{V}$) of a certain size z, the capture volume is approximated by a sphere of radius $r_{\alpha,z}$ around the object. Such an approach is certainly simplistic from an atomic-level point of view, because it associates to each defect an isotropic strain field, under the assumption that the medium is homogeneous and continuous. This approach is particularly problematic in the case of SIA loops, as discussed in Section 4. However, this is at present the widely accepted state-of-the-art [21–25]. Work is in progress to optimise the choice of the capture radii, within the limitations inherent to its use [62] and a sensitivity study is presented in this paper.

Table 2 summarises the description of the capture radii used in this work for each possible object, as a function of type and size. The ratio behind the formulae in Table 2 is that $r_{\alpha,z}$ must account for the volume occupied by the object, increased by an amount equal to the supposed extension of the corresponding effective strain field. The fact that SIA-type defect strain fields are larger than vacancy-type defect strain fields is taken into account by introducing a bias in the relevant radii: $r_{\mathrm{I}} = \gamma r_{\mathrm{V}}$, where $\gamma = 1.15$ is deduced from experimental results and corresponds to a fairly common choice [21,23,43]. Moreover, the capture radius for solute atom clusters is also a function of the object with which it is interacting (pure solute cluster or mixed vacancy-solute cluster), in order to account for the absence of binding energy between second nearest neighbour solute atoms, while vacancies do have a binding energy with solute atoms even when separated by larger distances (second nearest neighbour) [63,64].

The reaction distance is postulated to be the sum of the capture radii associated to the two interacting objects, A and B ($d_{r,\mathrm{A+B}} = r_{\mathrm{A}} + r_{\mathrm{B}}$): an interaction exists and a reaction occurs if the two objects are located at a distance less than $d_{r,\mathrm{A+B}}$.

Experimentally, the vacancy-SIA recombination distance is reported to vary between 2.2 and 3.3 lattice parameters in pure Fe, corresponding to ~100–300 atomic volumes in the spherical approximation [65,66]. Values of this order are generally adopted in the rate theory [43,67]. MD simulations with empirical potentials predict much smaller distances ($1.7a_0$ [68], $1.9a_0$ [22]). A particularly striking case of large disparity between experimental and MD values for the recombination volume is that of vanadium: while experimentally this is reported to be as high as 700 atomic volumes [69] atomistic simulations predict only about 140 atomic volumes [69]. This discrepancy remains unexplained. In most published OKMC studies a first or second nearest neighbour distance has been used as recombination distance [23,25], although also larger values ($1.9a_0$) have been proposed [22]. To our knowledge, the large experimental values have never been used in OKMC simulations. A sensitivity study to assess the influence of the choice of the recombination radius, extended up to the largest experimentally reported value for Fe, i.e. 3.3/2 lattice units, is presented in this work.

2.2.2. Diffusion parameters

The motion of the different objects is characterised by the attempt frequency and the migration energy, as in Eq. (1), which are the essential factors determining the diffusion coefficient. In sets A and C, only single SIA and single vacancies are mobile, as well as solute-vacancy pairs, thereby allowing solute migration. The corresponding diffusivity parameters are presented in Table 3. Note that set A employs the experimentally fitted values of Ref. [43], while set C adopts the same values as set B for single defects. The parameters chosen for set B are described and commented in what follows for each defect species and summarised in Table 4.

2.2.2.1. Self-interstitial atoms. The parameter choice adopted in set B to describe SIA and SIA cluster diffusivity is consistent with KMC models already published in Refs. [21–25] and based on a series of MD simulation studies of SIA and SIA cluster migration in Fe [21,56–60]. A constant attempt frequency, ν_0, equal to 6×10^{12} s^{-1} (see discussion of this value in the vacancy section), is made to decrease as a function of the cluster size m according to a power law (m^{-s}). MD results by Osetsky et al. [56] suggest a law close to $1/\sqrt{m}$ ($s = 0.51$) and this choice has been tentatively adopted in set B. Other MD studies provide larger exponents [60], but our model allows the rate of decrease to be freely tuned by changing

Table 2
Capture radii associated to different objects as a function of object size (expressed by the integer numbers n, m, p and q)

Object	Capture radius
mI $m \geqslant 1$	$r_{\mathrm{I},m} = \gamma\left[(r_0+\varepsilon) + \left(\frac{3}{4\pi}\frac{a_0^3}{2}m\right)^{1/3} - \left(\frac{3}{4\pi}\frac{a_0^3}{2}\right)^{1/3}\right]$
mV $m \geqslant 1$	$r_{\mathrm{V},m} = (r_0+\varepsilon) + \left(\frac{3}{4\pi}\frac{a_0^3}{2}m\right)^{1/3} - \left(\frac{3}{4\pi}\frac{a_0^3}{2}\right)^{1/3}$
mV + nS $m \geqslant 1$, $n \geqslant 1$	$r_{\mathrm{S},n+\mathrm{V},m} = (r_0+\varepsilon) + \left(\frac{3}{4\pi}\frac{a_0^3}{2}(m+n)\right)^{1/3} - \left(\frac{3}{4\pi}\frac{a_0^3}{2}\right)^{1/3}$
nS interacting with qS + pV object $n \geqslant 1$, $p \geqslant 1$, $q \geqslant 1$	$r_{\mathrm{S},n(\mathrm{V})} = \left(\frac{a_0}{2}+\varepsilon\right) + \left(\frac{3}{4\pi}\frac{a_0^3}{2}n\right)^{1/3} - \left(\frac{3}{4\pi}\frac{a_0^3}{2}\right)^{1/3}$
nS interacting with pS object $n \geqslant 1$, $p \geqslant 1$	$r_{\mathrm{S},n(\mathrm{S})} = \left(\frac{\sqrt{3}a_0}{4}+\varepsilon\right) + \left(\frac{3}{4\pi}\frac{a_0^3}{2}n\right)^{1/3} - \left(\frac{3}{4\pi}\frac{a_0^3}{2}\right)^{1/3}$
Traps	$r_{\mathrm{trap}} + \varepsilon$
Surface	$a_0/2 + \varepsilon$

In all sets (A, B and C) $r_0 = \sqrt{3}a_0/4$, i.e. half the first nearest neighbour distance (with $a_0 = 2.87$ Å), but sensitivity studies have been done with different values using set B. The bias factor for SIA is $\gamma = 1.15$. The capture radius for a solute cluster changes depending on whether it interacts with a mixed object (mS + pV) or another pure solute cluster (nS) and does not depend on r_0. In set B, traps interacting only with interstitials have a 5 Å r_{trap} value except when otherwise mentioned. Note that ε denotes an arbitrary, small, positive correction to the exact values.

Table 3
Sets A and C parameters for object migration (only single point defects are mobile)

	Attempt frequency ν (s^{-1})		Migration energy E_m (eV)		Exp. E_m (eV)
	Set A	Set C	Set A	Set C	
Single vacancy (V)	1.2×10^{15}	6×10^{12}	1.3[a]	0.69	0.55 [79]
V + nS; $n>1$	1.2×10^{15}	6×10^{12}	1.3[a]	0.69	
mV + nS; $m>1$	Immobile				
Single SIA[b] (I)	4.8×10^{11}	6×10^{12}	0.3	0.04	0.3 [70–72]
mI; $m>1$	Immobile				

$q = 10$.
[a] Effective value, implicitly including trapping effects.
[b] 3D random walk.

the value of the exponent s of m (see results in Section 3.2). On the contrary, the migration energy is fixed to 0.04 eV, for both single SIA and clusters thereof. The latter value, much lower than the experimental one for single SIA (0.3 eV [70,71]), is typically found in MD simulations [21,56–59].

Table 4
Set B parameters for object migration (clusters of all sizes are mobile)

	Attempt frequency ν (s^{-1})	Migration energy E_m (eV)	Exp. E_m (eV)	Comment
Single vacancy	ν_0	0.69	0.55 [79]	
V + nS	$\nu_0(q^{-1})^{n-1}$	0.69		
mV; $m > 1$	$\nu_0(p^{-1})^{m-2}$	0.69		
36mV + nS; $m > 1$, $n \geqslant 1$	$\nu_0(p^{-1})^{m-2}(q^{-1})^{n-1}$	0.69		
Single SIA	ν_0	0.04	0.3 [70–72]	3D motion
mI; $m > 1$	$\nu_0 m^{-s}$	0.04		1D motion along ⟨1 1 1⟩

The values of the constants are $\nu_0 = 6 \times 10^{12}$ s^{-1}, $p = 100$, $q = 1000$ and $s = 0.51$.

The SIA in Fe is known to have a ⟨1 1 0⟩ dumbbell configuration in its most stable configuration [70–72]. SIA clusters are conversely described as a collection of ⟨1 1 1⟩ crowdions, starting from size 2 [21,56–60]. MD simulations with empirical potentials show [21,56,58,59] that both single SIA and SIA-loop motion consists of a succession of glides along a ⟨1 1 1⟩ direction. In the case of the single SIA this is made possible by a relatively easy rotation from the ⟨1 1 0⟩ to the ⟨1 1 1⟩ configurations (~0.1–0.3 eV activation energy [22,58–60,73]). Single SIA can also easily change ⟨1 1 1⟩ glide direction, resulting in an almost fully 3D random walk, depending on temperature [57,59,74]. For SIA clusters the change of direction is increasingly less likely with size [73]. These features are introduced in the model by allowing single SIA and SIA clusters to move only unidimensionally along a ⟨1 1 1⟩ direction, while experiencing ⟨1 1 1⟩ direction changes with a probability that is assessed based on an activation energy for crowdion rotation, E_{a_rot}. The decision about the ⟨1 1 1⟩ direction change is made according to the standard MC algorithm, using the Boltzmann factor $\exp(-E_{a\_rot}/kT)$ as probability of occurrence.

In the present work single SIA are assumed to have a full 3D motion at all temperatures ($E_{a\_rot} = 0$), similarly to what has been done in most published OKMC studies [21,23–25]. SIA clusters of any size are constrained to follow a 1D ⟨1 1 1⟩ random walk, i.e. the ⟨1 1 1⟩ direction change is prohibited ($E_{a\_rot} = \infty$). The rational behind these choices is briefly discussed in Section 4. To give an idea of what would be the effect of allowing cluster rotation, if for instance E_{a_rot} was set to 1 eV for a SIA cluster (which is the case for sizes above 3 [73]), the probability of direction change at 300 °C would be around 10^{-9}, so that a net 1D motion is obtained in practice.

It should be noted that SIA may in principle play a role in Cu transport. Indeed mixed Cu-I objects were observed to form in the course of 20 keV cascades in Fe–2at.%Cu alloys [20] and have been experimentally deduced to exist [75]. However, MD simulations of mixed dumbbell migration that we performed for 400 ps at 300 and 800 K indicate that Cu is not transported by the SIA at the mentioned temperatures. The starting configuration is a mixed dumbbell in either a pure Fe lattice or a Fe–0.2%Cu matrix. After a few timesteps, the dumbbell releases the Cu atom and travels (as an Fe–Fe dumbbell) in the array. The Cu atom thus remains in the neighbourhood of its initial position. We calculated within the density functional theory, using the VASP code [76], the binding energy between an Fe–Fe dumbbell and a copper atom beside to be around 0.2 eV, without finding any positive binding energy for the mixed dumbbell configuration [63]. Thus, Cu atoms may affect slightly the SIA mobility by, for instance, inducing directional changes [77] or weak trapping at very low temperature, but this is probably not a first order effect and was hence not taken into account here. The possibility of interaction between dislocation loops and Cu precipitates or Cu-vacancy complexes is currently under study [78].

2.2.2.2. Vacancies. For single vacancies, the migration energy is taken to be 0.69 eV (as found with EAM potentials and close to the ab initio value of 0.65 eV [63] and the experimental value of 0.55 eV [79]). In the case of clusters, like for SIA, the migration probability is allowed to decrease with the vacancy cluster size (for size >2) by applying a geometric progression of common ratio p^{-1} to the constant attempt frequency ν_0, as shown in Table 4, while keeping the migration energy unchanged, in this following the suggestion of Ref. [80]. The value of ν_0 was set to 6×10^{12} s^{-1} after finding that this choice provided the correct self-diffusion coefficient for Fe in an AKMC simulation. In default of any similar procedure for SIA, the same value was extended, as a first approximation, to them as well.

2.2.2.3. Copper atoms. Substitutional solute atoms cannot move without the intervention of point defects. Since the formation and migration of Cu-SIA mixed dumbbells in Fe seems unlikely and copper has been shown to have a reasonably strong interaction with vacancies [63,64,81,82], these solute atoms in the model are allowed to diffuse only by forming mobile complexes

with vacancies, typically mixed copper-vacancy pairs, but also larger mobile complexes. This description is suggested from the analysis of AKMC simulations, showing that vacancy clusters and small Cu-vacancy complexes are indeed mobile as a whole up to appreciable sizes [1,26–28]. In the case of a Cu-vacancy pair, physically the mechanism corresponds to a situation where most of the vacancy jumps are exchanges with the same Cu atom or correlated jumps around the Cu atom, having the net effect of transporting the latter in the same direction as the vacancy for a time equivalent to the lifetime of the pair. For larger Cu-vacancy complexes the physical mechanism is more involved. For a complex to move as a whole, vacancies must move along its surface, producing collectively an effective motion. If Cu atoms are present, a higher number of vacancy jumps are required, because the Cu atoms must also move with the vacancies. These features are tentatively allowed for in the OKMC model by keeping the migration energy of the complexes equal to the migration energy of the single vacancy, with a prefactor that decreases following a geometric progression with not only the number of vacancies, but also the number of copper atoms (common ratio q^{-1} cf. Table 4). For an additional discussion of the mobility of Cu-vacancy complexes in OKMC and AKMC see Ref. [28].

2.2.2.4. Traps. The production of dislocation loops in pure Fe is often explained by assuming the presence of traps for point defects in the Fe matrix. These traps are generally associated with C or N atoms, which are known to affect point defect motion due to their binding energy with SIA or vacancies. For example, it seems now clearly established that the value of 1.28 eV for the vacancy migration energy obtained by Schaefer et al. [83] is due to the presence of a very small amount of impurity atoms [84]. This is in agreement with our ab initio calculations, predicting a 0.4 eV binding energy between a C atom and a vacancy [85]. However for SIA, also in the light of ab initio calculations [86], the situation is more complicated, and it is not completely clear whether the presence of impurities is the only source of trapping effects. This point is further discussed in Section 4. Therefore in the present model C and N atoms do not appear explicitly, and *generic*, immobile traps are included instead, acting on both vacancies and/or SIA. The defect-trap binding energy is used as an adjustable parameter. In the present model it is accepted that the same trap can catch more than one point-defect and point-defect cluster of each type.

2.2.2.5. Summary. To summarise, in sets A and C only single vacancies, single SIA and Cu-vacancy pairs are mobile (Table 3), whereas in set B also small defect clusters retain some degree of mobility, with an attempt frequency that decreases with their size according to laws adapted to each species, as shown in Table 4.

2.2.3. Dissociation events

For the emission from either a trap or an object, the activation energy E_a equals $E_m + E_b$, where E_b is the binding energy of the emitted object to the emitting cluster. There exist very few experimental data about these binding energies. To our knowledge, the only available value of this type from experimental measurements, of relevance for this work, is the Cu/single-vacancy binding energy: 0.14 eV [81] or 0.11 eV [82].

In our model, both the emission of a single-vacancy and a vacancy-Cu pair from vacancy and vacancy-solute clusters are possible. The binding energies were computed in detail using molecular statics [20] up to 10 vacancies and 5Cu atoms and then fit to a law, in the spirit of Soneda's work [21] and Barbu's law [43]:

$$E_b((m-a)\mathrm{V}+(n-b)\mathrm{Cu}, a\mathrm{V}+b\mathrm{Cu}) = E_{for} + (E_{b2}-E_{for})\left[\frac{m^{2/3}-(m-1)^{2/3}}{2^{2/3}-1}\right], \quad (5)$$

where $(a,b) = (1,0)$ for vacancy emission and $(a,b) = (1,1)$ for vacancy-Cu pair emission. This formula was derived so as to give, for the vacancies, the divacancy binding energy for $m = 2$, and the vacancy formation energy for $(m \to \infty)$, as very large clusters can be considered to be equivalent to a free surface. In (5) Cu is postulated not to affect the vacancy binding energy value. This is of course an approximation. However, detailed calculations of the binding energy of a vacancy to Cu-vacancy complexes [87,88] revealed that, although not totally negligible, the effect of the presence Cu atoms on this magnitude is very weak, all the more for large complex sizes. A study of the difference between adopting the approximation in Eq. (5) and using more properly calculated binding energies is underway [89].

Table 5 presents the parameters to be inserted in formula (5) to obtain the binding energies used in this work to simulate Fe–Cu alloys. $E_b((m-1)\mathrm{V} + n\mathrm{Cu},\mathrm{V})$ is the binding energy of a vacancy to a cluster containing $m-1$ vacancies and nCu atoms, i.e. the energy needed to remove a vacancy from a cluster containing m vacancies and nCu atoms. $E_b((m-1)\mathrm{V} + (n-1)\mathrm{Cu},\mathrm{VCu})$ is the binding energy of a vacancy-Cu pair with a cluster containing $m-1$ vacancies and $n-1$ Cu atoms, i.e. the energy needed to remove a Cu-vacancy complex from a cluster containing m vacancies and n Cu atoms. Finally, $E_b((m-1)\mathrm{V},\mathrm{V})$ is the binding energy of a vacancy to a cluster of $(m-1)$ vacancies (e.g. for a di-vacancy $E_b(2\mathrm{V},\mathrm{V})$).

The dissociation of SIA clusters is a rare event because they have a high binding energy, as observed by Schilling [90] and confirmed by MD simulations

Table 5
Constants used in formula (4) for the calculation of the binding energies of different elementary defects to clusters of different sizes and binding energy to traps

Object	E_{b2} (eV)	E_{for} (eV)
$E_b((m-1)V,V)$	0.2	1.6
$E_b((m-1)V + n\text{Cu},V)$	0.2	1.6
$E_b((m-1)V + (n-1)\text{Cu},\text{VCu})$	0.1	1.88
$E_b(m\text{V} + (n-1)\text{Cu},\text{Cu})$	Not considered in this work	
$E_b((m-1)I,I)$	1.0	4
Traps for SIA (independent of cluster size)	$E_b = 0.9$[a]	//

[a] Except when otherwise mentioned. In set A and C, traps are implicit in the choice of the diffusivity laws.

[56,60]. They are therefore very stable against dissociation. Nevertheless, this event is taken into account and described using a formula like (4) as well, with the parameters indicated in Table 5. Such a dissociation is anyhow seen to be effective only for very small clusters (di- and tri-interstitials).

2.3. Statistical treatment

MC simulations are inherently stochastic. Strictly, one single simulation is in principle meaningless and only by performing a statistical treatment on several parallel simulations, each of them following a different sequence of random numbers, is it possible to draw conclusions on the physical trends. This problem is particularly important when the evolution of one single external event (a single displacement cascade) is studied. When many external events are superposed, distributed in time according to a probability of occurrence (dose rate), as is the case of irradiation simulations, this problem is less important because an averaging effect is naturally obtained by randomly choosing the event from a database of different cascades (in the case of neutron and ion irradiation) or introducing randomly distributed Frenkel pairs (in the case of electron irradiation).

The evolution of the system during a single cascade ageing simulation has been described in this work by selecting a set of indicators of physical interest, output at each time decade (i.e. at, say, 10^{-9}, 10^{-8} s,...). These indicators are the number and mean size of the different types of objects, the fraction of single point defects and point defects in cluster and the atomic percentage of solute atoms in the precipitates and in the matrix. Generally, we performed 50 cascade ageing simulations from the same initial configuration, with different random number seeds, to produce, for each time-decade, a column of 50 values for each indicator. All these columns have been treated statistically not only to get the mean value of the indicator and the spread around the mean at each decade (error bar), but also to establish on statistical grounds, if needed, whether two apparently similar results should be really considered the same or not. This comparison can be done by using standard *F*-test, *t*-test and ANOVA tests, as described in any introductory statistics book.

3. Results

3.1. Cascade ageing

In this section we present the main results of a work of comparison between different KMC parameter sets, conducted on a set of both MD and binary collision approximation (BCA) displacement cascades, initiated in Fe and Fe–0.2%Cu by a 20 keV PKA. The MD cascades belong to a database already discussed in previous work [19,20]. The BCA cascades were produced using the code MARLOWE [91], after tuning its parameters in order to obtain results as close as possible to the MD simulations, in terms of volume of the cascade, anisotropy and number of Frenkel pairs [68]. The similarity between cascades was assessed using the component analysis [92]. A first study on the effect of using MD or BCA cascades as a primary damage source for ageing simulations with KMC is presented elsewhere [38] and a more complete study is underway [93]. Here the focus is on the effect of the use of different parameter sets for the simulation of the same phenomenon. All simulations were performed at the same temperature, namely 600 K (close to temperature of operation of RPV) in a $100a_0 \times 100a_0 \times 100a_0$ simulation box. Studies at different temperatures are presented in Section 3.2.

Fig. 2 shows a representative plot of the evolution in time of the number of SIA and vacancies during the ageing of a 20 keV displacement cascade in Fe–0.2%Cu in a box with absorbing boundaries using set B. In the first 10^{-7} s, recombination between vacancies and SIA, formation of SIA clusters and SIA leaving the simulation box are observed. Subsequently, vacancies start diffusing: some of them leave the box as single-vacancies, while others form clusters, including or not solute atoms (not indicated in the figure). These clusters retain some mobility and finally leave the box. The contribution to cluster disappearance via vacancy emission appears to be small, at least at the temperature at which the simu-

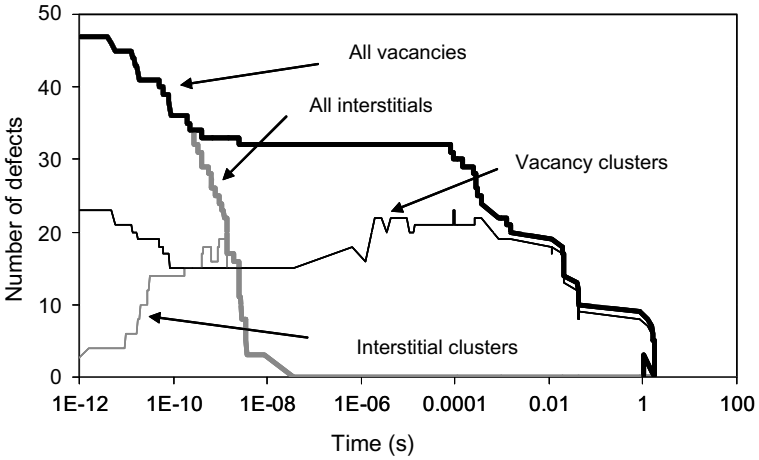

Fig. 2. Example of evolution in time (logarithmic scale) of the number of SIA (grey) and vacancies (black), both total (thick line) and in cluster (thin line), during the ageing of a 20 keV displacement cascade in Fe–0.2%Cu.

lation was performed. The time scale of these events is spread over about 13 decades.

3.1.1. Effect of migration energies and mobilities

In Fig. 3, the example of a 20 keV MD cascade aged in pure Fe (a) and Fe–0.2%Cu (b) using the three different parameter sets, described in Tables 1–5, is reported. The average clustered fraction of point defects as a function of time (by decades) is shown. The error bars correspond to the standard deviation. All curves are interrupted when statistics become too poor. Full symbols denote the evolution of the percentage of SIA in clusters; open symbols the same for vacancies.

According to sets B and C (SIA migration energy 0.04 eV), new SIA clusters start to form already at 10^{-13} s, reaching a peak value after, respectively, 10^{-10} and 10^{-9} s. With set A (SIA migration energy 0.3 eV), clustering starts only after 10^{-10} s and reaches the peak value at 10^{-6} s. After the peak value is reached, sets A and C (only single defects mobile) exhibit essentially the same behaviour: a long plateau of surviving, immobile SIA in clusters, that can only disappear by progressive 'erosion' via annihilation with single vacancies. The descent starts, respectively, at about 10^{-5} and 10^{-2} s, which correspond to the onset of massive single vacancy migration according to the two different migration energy choices. Using these two parameter sets, a residual fraction of SIA in clusters remains in the simulation box till the end of the simulation, because once all single vacancies have annihilated with SIA clusters, further SIA disappearance can only occur through vacancies emitted from clusters, which is a much slower process. Conversely, set B, which allows all SIA clusters to move with a low migration energy, although with decreasing attempt frequency, predicts a rapid disappearance of all SIA clusters within 10^{-8} s, i.e. long before the single vacancy migration onset. Therefore, according to this set the kinetics of SIA and vacancies are clearly separated. Note that, even in relatively high dose-rate cascade irradiation conditions, such as self-ion implantation ($\sim 10^{-4}$ dpa/s) or high-flux test reactors ($\sim 10^{-6}$ dpa/s), in a $100a_0 \times 100a_0 \times 100a_0$ simulation box a second cascade will only appear after $\sim$1 s or more. Therefore, from the point of view of intercascade interaction and damage accumulation effects, it is mostly the last part of the cascade ageing simulation that should be looked at. This means that, without traps, almost independently of the assigned migration energy ($\leqslant$0.3 eV), no SIA cluster will remain in the box with set B, even under high flux irradiation conditions.

As a consequence of the absence of interaction between SIA and solute atoms, the difference between pure Fe and Fe–0.2%Cu in the SIA clustered fraction is negligible. Yet, the effect of the presence of Cu on the clustered fraction of vacancies (open symbols) is clear. The peak amount of vacancies in cluster is significantly larger, with little or no difference from one parameter set to the other, because all share the same binding energy values from Eq. (5) and the same capture radius (see Section 3.1.2). The high peaks that characterise the vacancy clustered fraction evolution pattern in Fe–0.2%Cu appear at the onset of single-vacancy migration. They correspond to a large amount of mobile (in all three parameter sets) Cu–V pairs, formed by the migrating single vacancies which, in the absence of Cu atoms, would be leaving the box or, in some cases, increasing the size of existing clusters. However, Cu has little or no effect on the kinetics: sets B and C (same migration energy for vacancies, 0.69 eV), predict vacancy clustering, after a slight depletion due to recombination, at

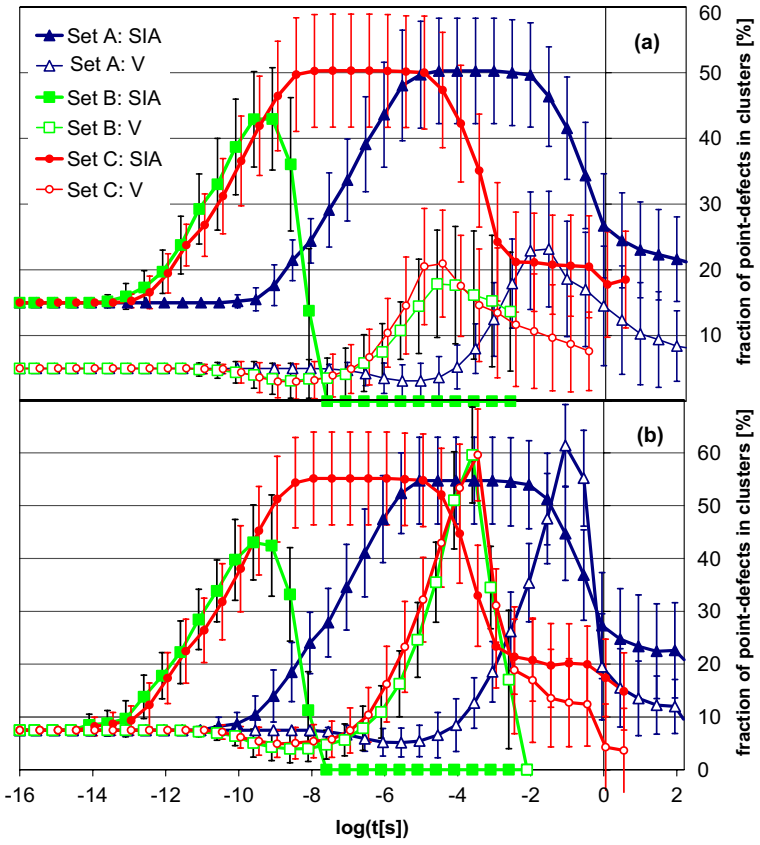

Fig. 3. Evolution in time (logarithmic scale) of the average clustered fraction of both SIA (full symbols) and vacancies (open symbols) for the same 20 keV MD cascade, aged in pure Fe (a) and Fe–0.2%Cu (b) using the three different parameter sets described in Tables 1–5. The error bars correspond to the standard deviation.

10^{-7} s. The peak of clustered fraction is reached at, respectively, 10^{-5} s without Cu and 10^{-4} s with Cu. The main difference between B and C is that, because of the mobility of vacancy and Cu-vacancy clusters, set B predicts no residual amount of vacancies left at the end of the simulation. With set A, as a consequence of the larger migration energy (1.3 eV), the curves are shifted in time by about three decades. Overall, it can be said that the 'intermediate' parameter set C provides predictions analogous to set B in the case of vacancies and set A in the case of SIA.

In Fig. 4 three groups of curves, corresponding to the evolution in time of the fraction of Cu atoms remaining in the matrix after ageing a number of cascades, are displayed for the three parameter sets A, B and C. No real precipitation occurs, because one single cascade does not provide a large enough amount of vacancies to allow such an event. However, Cu–Cu pairs and sometimes also Cu–Cu–Cu triplets, initially purposefully absent, are seen to appear and this is a clear hint that nuclei of future precipitates are starting to be generated. Differences between parameter sets are visible. Sets A and C, with only single point defects (and Cu-vacancy pairs) mobile, lead to more Cu aggregation than set B (clusters of all sizes mobile). This can be rationalised because in sets A and C the absence of mobile clusters forces the emission of single vacancies or of Cu–V pairs to become a more frequent event, thereby enhancing the possibility that Cu atoms are further transported to form precipitate nuclei. Conversely, in set B mixed complexes are mobile and can more easily further grow in size, but are globally less efficient in transporting Cu atoms. Thus, a larger number of Cu–Cu pairs, containing most of the Cu atoms subtracted from the matrix, is produced with sets A and C. On the contrary, with set B most Cu atoms subtracted from the matrix appear to be part of small mixed clusters. At the end of the cascade ageing the vacancy clustered fraction is roughly the same with and without Cu (Fig. 3), but the mean cluster size (not shown) is different. In pure Fe slightly larger vacancy clusters (mean size 3 ± 2) are formed than in Fe–0.2%Cu (mean size 2 ± 1), because in the alloy the same

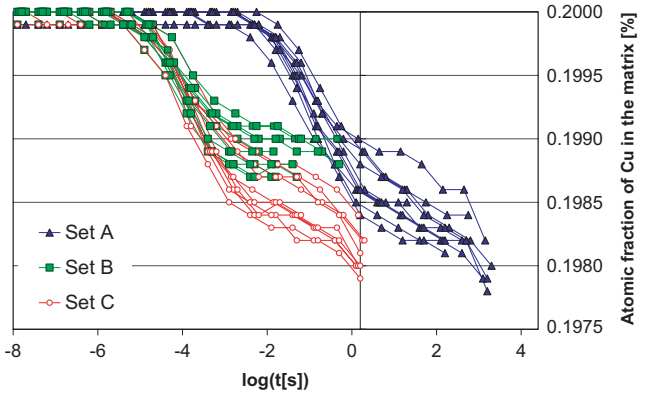

Fig. 4. Evolution in time (logarithmic scale) of the average atomic fraction of Cu atoms in the matrix for a group of ten 20 keV BCA cascades, aged in Fe–0.2%Cu ($100a_0 \times 100a_0 \times 100a_0$ simulation box) using the three different parameter sets described in Tables 1–5.

number of vacancies is distributed in a globally higher number of clusters, most of them mixed (containing 1 or 2 Cu atoms), particularly with set B.

In summary, a comparison between sets A, B and C, performed for a large set of cascades with proper statistical treatment, reveals that the choice of point defect migration energy clearly affects the time required for clustering onset. The fact that only single point defects are mobile has a visible effect on SIA clustering kinetics, but not so much on vacancy clustering, because at any rate peak clustering depends mostly on the mobility of single vacancies. However, keeping only single point defects mobile seems to be the only way of predicting some residual damage (particularly SIA) remaining in the box at the end of the annealing. In order to have the same effect with set B, generic traps should be included (see Section 3.2). Furthermore, sets A and C allow more Cu agglomeration. The presence of Cu and the existence of a Cu-vacancy binding energy influences dramatically the amount of vacancy clustering at peak with all parameter sets. At the end of the ageing, all vacancies remaining in the box are contained in mixed clusters, independently of the parameter set.

3.1.2. Effect of capture radius

In this section we present the results obtained by ageing a 20 keV MD cascade in pure Fe and Fe–0.2%Cu using set B, with growing values of the r_0 parameter that defines the capture radii according to Table 2. Namely, r_0 has been set equal to half the first, second and third nearest neighbour (nn) distance in bcc Fe, as well as equal to $1.9a_0/2$, $2.2a_0/2$ and $3.3a_0/2$. Thus, the involved objects will react when they find themselves at a mutual distance of first, second and third nn, as well as $1.9a_0$ [22], $2.2a_0$ [66] and $3.3a_0$ [65] (or larger, if the SIA bias factor of Table 2 is allowed for). The latter two values correspond to the experimental assessment of the SIA-vacancy recombination radius in Fe.

In Fig. 5 the average clustered fraction of point defects versus time is represented, the error bars corresponding to the standard deviation. Fig. 5(a) refers to pure Fe, Fig. 5(b) to Fe–0.2%Cu. The effect of changing the capture radius on the clustered fraction of point defects is especially visible at the beginning: the larger the capture radius, the higher the number of identified clusters. The initial mean size of the clusters is found to be ~2 for vacancies and ~3 for SIA, independently of the choice of the radius. In the course of the simulation the behaviour of the curves can also be considered very similar: radii differing by a factor ~4 produce peak point-defect clustered fractions that differ by only a factor 1.5. Interestingly, while the peak vacancy clustered fraction in pure Fe is higher for larger radii, as it seems logical, the reversed trend is observed in Fe–Cu. The explanation of this effect involves looking at other characteristic magnitudes describing the cascade ageing.

In Fig. 6 the other two fractions of point-defects, namely *disappeared* (a) and *single* point-defects (b), are plotted versus the logarithm of time in the case of pure Fe. The kinetics of SIA is much faster than the kinetics of vacancies. In the case of SIA three processes occur in sequence, but almost simultaneously: clustering, recombination with vacancies and migration to sinks (box boundaries). Despite the initial differences, the SIA evolution is largely independent of the choice of the capture radius. At 10^{-8} s no more single SIA remain in the box and the recombination phase ends. At that point, on average, it is found that about 2–3 SIA clusters, of size $\sim 4 \pm 2$ for smaller radii and $\sim 5 \pm 2$ for larger radii, remain in the box and promptly leave it. In the case of vacancies it is possible to distinguish from Fig. 6(a) two distinct phases of disappearance. The vacancies disappeared between, roughly, 10^{-12} and 10^{-8} s are those that annihilated with SIA. After that time no more SIA remain in the box and vacancies start moving and clustering. Only from 10^{-4} s a second phase of vacancy

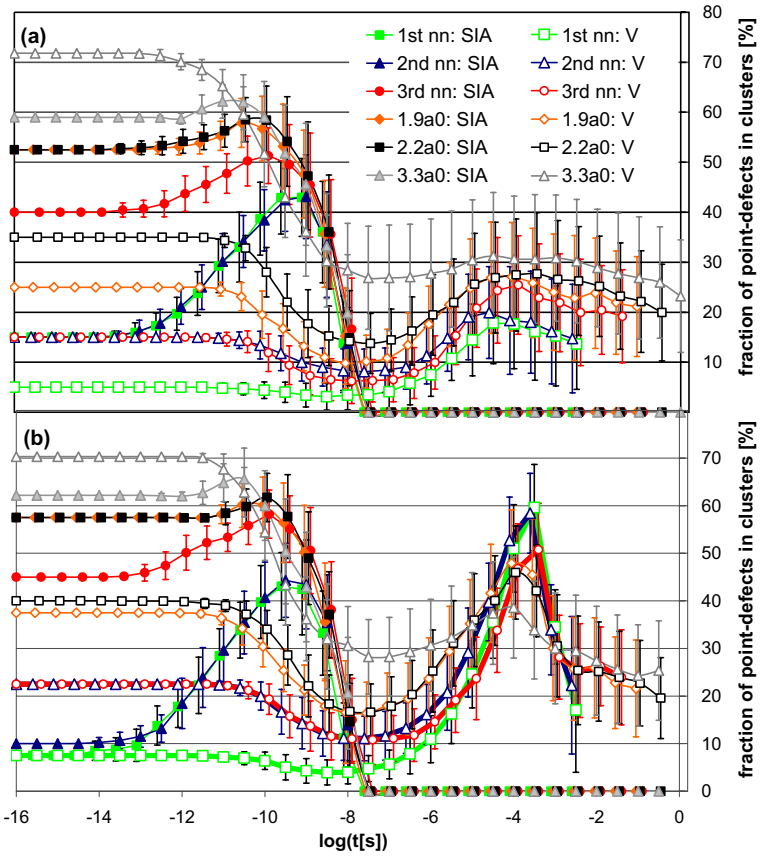

Fig. 5. Evolution in time (logarithmic scale) of the average clustered fraction of both SIA (full symbols) and vacancies (open symbols) for the same 20 keV MD cascade, aged in pure Fe (a) and Fe–0.2%Cu (b) using set B, with different values for the recombination distance.

disappearance is detected, corresponding to (single) vacancies reaching the boundaries. Therefore, the plateaux in Fig. 6(a) quantify the fraction of annihilated point-defects, varying from less than 40% with small radii up to ~60% with the largest radius. Most or all of the vacancies reaching the boundaries shortly after 10^{-4} s are single-vacancies. The fraction of vacancies in clusters corresponds, roughly, to the fraction of vacancies remaining in the box at the end of the annealing, when a second cascade has some probability of being produced in the same volume under irradiation. This fraction, as noticed (Fig. 5), is only weakly dependent on the choice of the radius and varies between ~15 and ~30% for growing radii in pure Fe. Thus, the main effect of the choice of the radius is on the quantity of *freely migrating single-vacancies* emitted from the cascade region, which can vary between ~40% of the initial amount for the smallest radius and ~10% for the largest radius. Taking into account that, roughly, the initial number of vacancies corresponds to 0.3 times the NRT number of displacements per cascade [7,17–20,34], these two extreme percentages of free vacancies correspond, respectively, to ~12% and ~3% of the NRT. While the latter value is closer than the former to experimentally deduced fractions of freely migrating defects in pure elements [94], both are in fact in the correct range and consistent with experimental assessments [95] and previous simulation work [21,22].

The different excess of single-vacancies depending on the choice of the radius explains also why the clustered fraction peak is smaller in Fe–0.2%Cu for larger radii (Fig. 5(b)). That peak is due to single-vacancies migrating towards the boundaries which encounter solute atoms, thereby forming Cu–V pairs. Larger radii produce less single vacancies and therefore lower peaks of small mixed clusters.

Two more effects of the choice of the capture radius in Fe–Cu have been detected. They are illustrated in Fig. 7, where the average number of vacancies in *mixed* clusters (a) and the average number of Cu atoms in clusters containing *only Cu atoms* (b) are plotted versus the logarithm of time. The first effect is that larger capture

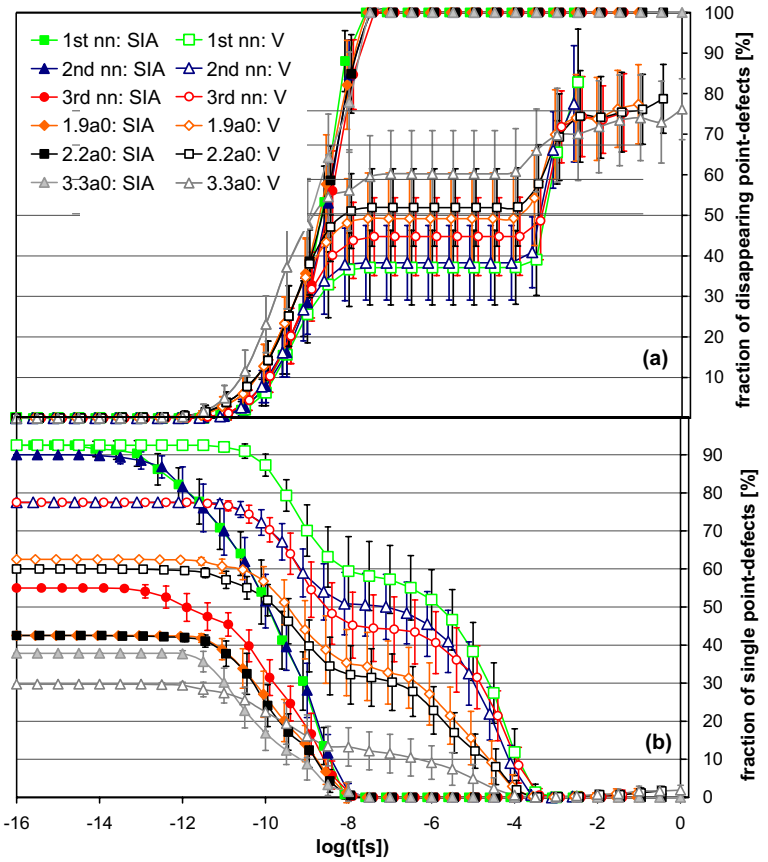

Fig. 6. Evolution in time (logarithmic scale) of the average fraction of disappeared (a) and single (b) point-defects in pure Fe (SIA: full symbols; vacancies: open symbols) using set B, with different values for the recombination distance.

radii lead to a larger mean number of vacancies in mixed clusters. Note that, on the contrary, the number of Cu atoms in mixed clusters is largely insensitive to the choice of the radius and remains close to 1 at the beginning, getting closer to 2 at the end of the cascade annealing. The enhanced absorption of vacancies in mixed clusters is ascribable to higher probability of cluster coalescence for larger interaction radii. In addition, the excess of fast-migrating single vacancies with small radii subtracts potential vacancies to mixed clusters (at the end of the annealing, invariably all clusters remaining in the box are mixed). The other effect of larger radii is to enhance Cu precipitate nucleation (Fig. 7(b)). A mean Cu cluster size closer to 2 reflects indeed a higher number of produced Cu–Cu pairs. The behavior of the largest radius is visibly different from the other cases because Cu–Cu pairs appear earlier. This happens because this radius is the only one leading to the identification, at the beginning of the simulation, of mixed clusters containing more than two Cu atoms, e.g. Cu_3–V complexes. The escape of Cu–V pairs from these complexes and/or the annihilation of the vacancy of these triplets with SIA leads to the formation of Cu–Cu pairs much earlier than with any other radius choice. Eventually, the largest radius allows the formation of ~104 Cu–Cu pairs.

In summary, the choice of the capture radius does affect the results of the cascade annealing. However, the effects are evident for some magnitudes, much less for others and, globally, less dramatic than expected. Larger radii promote recombination and reduce the amount of freely migrating single-vacancies, while producing somewhat larger clusters. Indirectly, larger radii also enhance Cu precipitate nucleation. However, the kinetics is essentially not influenced by the choice of the radius and differences become clearly visible only when comparing largely different radii. We checked that these conclusions hold for all sets of parameters.

3.2. Damage accumulation

In the previous section it has been shown that the choice of the capture radius does not have particularly dramatic effects on the damage state at the end of a cascade annealing. On the contrary, the recipe used for the

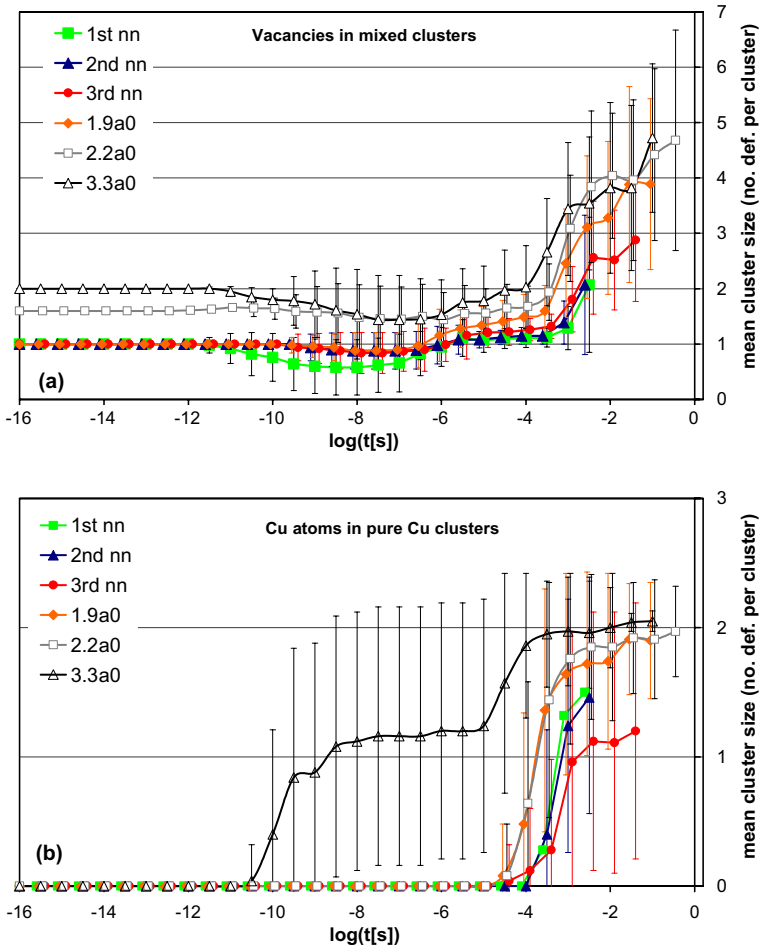

Fig. 7. Evolution in time of the average number of vacancies in mixed clusters (a) and Cu atoms in clusters containing only Cu atoms (b), in Fe–0.2%Cu, simulated using set B, with different values for the recombination distance.

description of the mobility of point-defects and point-defect clusters influences both the kinetics and the outcome of the cascade ageing. In particular, the strict requirement of allowing only single point defects to migrate seems to be, at first glance, the only way of keeping some residual damage in the box at the end of the ageing, despite the evidence of cluster motion from MD simulations [21,56–60]. Since damage is known to accumulate in Fe alloys under irradiation [1–5,43–50,84], this suggests that trapping mechanisms, either explicit (addition of traps in set B), or implicit (sets A and C) are fundamental for a correct prediction of radiation effects in these alloys. In the present section we propose a selection of simulations of irradiation experiments in pure Fe and Fe–Cu, aimed demonstrating that, provided that traps are introduced and with a choice of other parameters based mostly on MD simulation results, it is possible to obtain physically acceptable results from OKMC simulations, within the assumptions described in Section 2.

3.2.1. Neutron irradiation of pure Fe

Irradiation under cascade damage conditions, such as with neutrons, corresponds to a particularly complicated situation to model, because of the inhomogeneity in space and time of damage production. This complexity is however suitably reproduced in a KMC simulation of an ongoing irradiation, because new cascades can be easily introduced in different positions, according to a defined dose-rate, in a simulation box in which previous cascades are already more or less advanced in their annealing process, depending on the irradiation temperature.

Recently, a positron annihilation study on high-purity Fe specimens, neutron irradiated in the range of about 0.0001–0.8 dpa in the HFIR reactor at Oak Ridge National Laboratory, has been published [49,50]. This work provides an experimental assessment of the density and size distribution of vacancy clusters (nanovoids) versus dose in Fe which is extremely valuable for the val-

idation of OKMC models. In the same work, the total density of visible clusters (mostly interstitial clusters) versus dose is provided. Similar data could be also found in Ref. [46].

A dose-rate corresponding to HFIR ($\sim 10^{-6}$ dpa/s) was used for OKMC simulations where 0.23 dpa were accumulated at 70 °C in a $200a_0 \times 200a_0 \times 200a_0$ pure Fe box, with periodic boundary conditions. This equals the dose up to which results of void size distribution are provided in [49]. The HFIR spectrum was decomposed into 3×10^{16} Frenkel-pairs $cm^{-3}s^{-1}$, 4×10^{14} 10 keV cascade-debris $cm^{-3}s^{-1}$ and 2×10^{14} 20 keV cascade-debris $cm^{-3}s^{-1}$, in accordance with INCAS package results [33]. The simulation was first performed using set A, set B and set C. For set B, when no traps are introduced, no damage accumulation takes place. For set A and C, the saturation versus dose is clearly not reproduced (Fig. 8(a)). It appears thus that one needs to allow cluster migration and the introduction of traps to reproduce these experimental results. The influence of the capture radius was tested using set B with traps for SIA and their clusters, in a concentration of 100 ppm and with a binding energy between trap and object of 0.9 eV, and a capture radius for traps of 5 Å. Three different

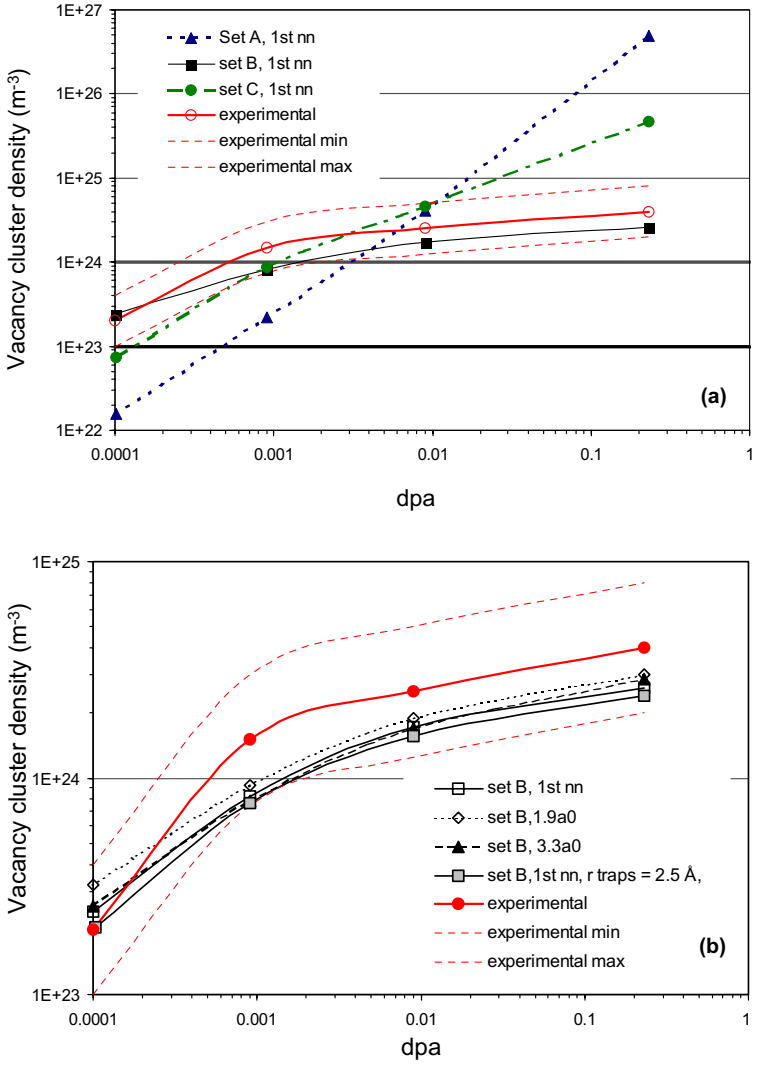

Fig. 8. Density of vacancy clusters in pure Fe at different doses after a neutron irradiation in HFIR, at 70 °C, including experimental uncertainty, as reported in Refs. [49,50], compared with OKMC simulations using (a) the three different sets (b) set B with traps for interstitials (binding energy of 0.9 eV and capture radius of 5 Å) for three different recombination distances. Set B with traps for interstitials with a binding energy of 0.9 eV and a capture radius of 2.5 Å is also represented on the figure. ($200a_0 \times 200a_0 \times 200a_0$ simulation box, periodic boundary conditions).

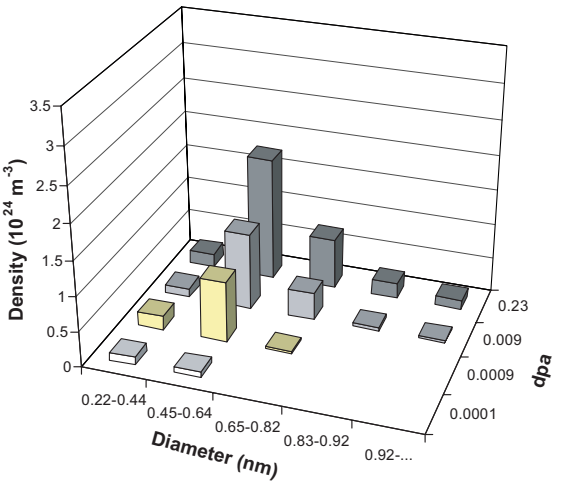

Fig. 9. Vacancy cluster size distribution versus dose according to the OKMC simulation using set B with traps and a 1 nm recombination distance. The size for a cluster of N vacancies is given by an equivalent diameter, i.e. the diameter of a sphere with a volume equal to N vacancies. To be compared with experimental results in Refs. [49,50].

recombination distances for the objects were chosen (namely first nn distance, $1.9a_0$ [22] and $3.3a_0$ [65]), thereby spanning the whole range of possibilities. Fig. 8(b) shows in this case excellent agreement between the results of the simulation and the vacancy cluster density measured by Eldrup et al. [49]. The choice of the radius proves to have very limited effect on the results, which are not distinguishable at high dose, although at low dose the smallest radius provides the best trend curve, fully contained in the experimental error bar. The capture radius and binding energy of the traps do not appear to have a very strong effect either, as can be seen Fig. 8. In Fig. 9 the vacancy cluster size distribution versus dose obtained from the simulation with set B and the smallest capture radius is shown. This figure can be directly compared with Fig. 4 in [49] and Fig. 6 in [50]. Again, the agreement between simulation and experiment is excellent. The only noticeable difference between simulation results and experimental measurements is that the former tends to shift the size distribution towards somewhat larger clusters (even using the smallest capture radius!), thereby predicting slightly lower density. The total density of clusters (mainly of interstitial nature) from TEM studies reported in [49,50] is compared in Fig. 10 with the density of visible ($N > 70$ [24]) SIA clusters from the simulation with set B with traps and the smallest capture radius. On the same figure, broadly homogeneous data from Ref. [46], obtained in a similar range of temperature after irradiation of pure Fe with both neutrons and protons, are also indicated, to give an idea of the experimental uncertainty. The simulation provides broadly correct orders of magnitude for cluster density, although in this case the trend is not as nicely reproduced as in the case of vacancy clusters. The prediction of the simulation resembles a step-like function, which correctly reproduces the need of an incubation dose to observe clusters by TEM in Fe, but seems to fail in yielding the correct density increase with dose.

3.2.2. Neutron irradiation of Fe–Cu alloys

RPV irradiation conditions correspond to a rather extreme case because only about 0.1 dpa are accumulated in about 30–40 years at ~300 °C in the material, under cascade damage conditions. This corresponds to an extremely low dose rate, of the order of 10^{-11} dpa/

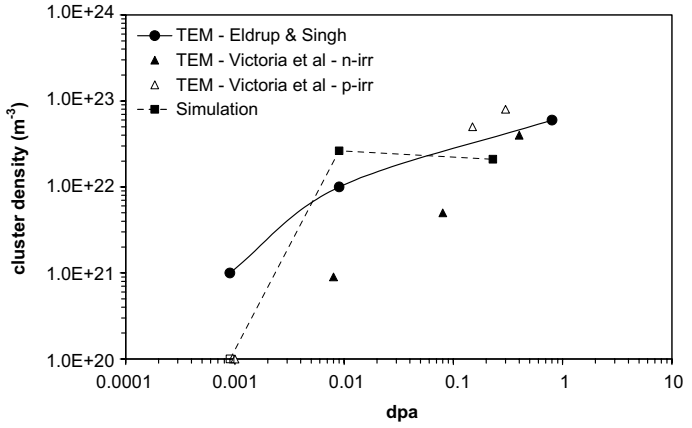

Fig. 10. Total cluster density versus dose in pure Fe from TEM studies [46,49,50] compared to SIA cluster density OKMC predictions using set B with traps (binding energy of 0.9 eV and capture radius of 5 Å) and a 1nn recombination distance. SIA clusters are supposed to become visible above size 70. The first simulation point should be read as density *lower than* 10^{-20} m^{-3}.

s, or lower with growing distance from the core. In order to test the OKMC model for low dose-rate irradiation conditions and for the prediction of Cu precipitation, simulations with a HFIR input flux divided by 10^5 ($\sim 10^{-11}$ dpa/s), up to 0.18 dpa at 300 °C, were conducted in a $100a_0 \times 100a_0 \times 100a_0$ Fe–Cu box with periodic boundary conditions, using again set B with traps and three possible capture radii. The results are shown in Fig. 11 in terms of percentage of precipitated Cu. In the absence of precise experimental results for Fe–Cu alloys irradiated in these conditions to compare with, we used tomographic atom-probe (TAP) data obtained from both Fe–Cu alloys and a collection of steels, irradiated at RPV operation temperature in test reactors, with dose-rates ranging from 10^{-5} to 10^{-8} dpa/s [5]. The advantage of these data is that they concern steels from dismantled reactors, for which data from real RPV conditions are available and no significant dose-rate effect has been observed [96]. Since the experimental data correspond to variable copper concentrations with a maximum around 0.2%Cu [5,96,97], two indicative copper concentrations have been considered in the simulation: 0.1% and 0.2%. The results obtained are in quite good agreement with the experimental data. The evolution of the fraction of Cu in precipitates saturates after ~0.03 dpa, as experimentally observed. At a dose of 0.1 dpa, the Cu clusters are rather small and the maximum size of Cu clusters is ~30 atoms (less than 1 nm) for the smallest recombination radius and ~150 atoms (~1.5 nm) for the largest one. Increasing the capture radius increases the fraction of Cu in precipitates, as already observed in the cascade annealing studies. However, the simulation results obtained with the three radii remain within the experimental error. With such a low dose rate, according to the simulation neither vacancy nor interstitial clusters remain in the simulation box: vacancy clusters evaporate and annihilate with SIA clusters between two incoming cascades (the average time between two cascades is 10^7 s in a $100a_0 \times 100a_0 \times 100a_0$ simulation box at this dose-rate!).

3.2.3. Electron irradiation

Electron irradiation experiments are typically used to study fundamental radiation effects, because of the absence of cascade damage production. The physical problem is hence simplified and for this reason experiments of this type are often used to benchmark radiation damage evolution models. However, it is a priori not guaranteed that models that correctly describe electron irradiation can be extended to neutron irradiation, or the other way round. Barbu and co-workers recently published the results of a series of modelling-oriented electron irradiation experiments in Fe alloys, used to validate the rate theory model by which set A was inspired [43]. In a high voltage electron microscope, thin foils (300 nm thickness) of pure Fe were irradiated under a high energy electron flux of $1.5\ 10^{-4}$ dpa/s for 1200 s at different temperatures and the final density of interstitial dislocation loops was measured in each case. This type of experiment is suitable to be simulated using an OKMC model. Fig. 12 shows the total density of dislocation loops (without distinguishing between $1/2\langle 1\ 1\ 1\rangle$ and $\langle 1\ 0\ 0\rangle$ type) versus temperature found in the experiments [43] and the corresponding computer simulation results (criterion of visibility: size $\geqslant 70$ [24]). Although the SIA cluster density is overestimated by the simulation, the temperature trend is broadly reproduced by set A, except for high temperature, and even better reproduced, with saturation at low temperature, by set B with 100 ppm traps for SIA and their clusters. Note, however, that in order to have the best agreement possible with set B, a value of the parameter s of Table 4

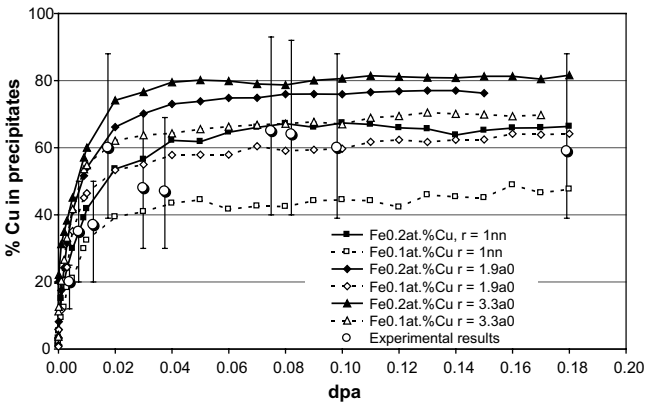

Fig. 11. Simulation of the evolution of the atomic fraction of precipitated Cu versus fluence for two dilute Fe–Cu alloys (0.1 and 0.2%Cu) neutron irradiated with a flux corresponding to HFIR/10^5 in a $100a_0 \times 100a_0 \times 100a_0$ simulation box, at 300 °C. Simulations done with set B with traps (binding energy of 0.9 eV and capture radius of 5 Å) and a 1nn recombination distance. The experimental data are from Auger et al. [5] and references therein [96,97].

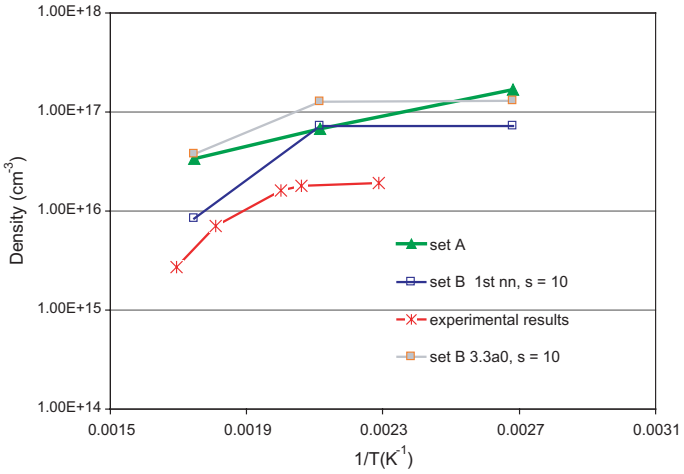

Fig. 12. Arrhenius plot of the number density of SIA clusters after a 1200 s electron irradiation in a $100a_0 \times 100a_0 \times 1000a_0$ pure Fe thin foil, as simulated using the parameter set A, as well as with set B with 100 ppm SIA traps ($E_{b,traps} = 0.9$ eV and s from Table 4 set equal to 10, as well as $r\_trap = 5$ Å). For set B two recombination distances were used, first nearest neighbour and $3.3a_0$.

equal to 10, instead of 0.51, had to be used, otherwise no interstitial clusters form at high temperature. This higher value of s corresponds to a much faster decrease of the mobility of SIA clusters with size than expected from MD simulations and is tantamount to considering essentially immobile large clusters, as proposed by other authors [25]. Note also that the smallest capture radius provides the closest agreement with the experiment.

4. Discussion

We have shown that our KMC model can produce results in fairly good agreement with experimental results. Yet, this model is somewhat rough and certainly needs further improvements. The weakest part of the present model concerns the description of the properties of SIA and SIA clusters. In particular, the description of the mobility is affected by some uncertainties, testified, among other things, by the need of tuning the s parameter of Table 4 to reproduce electron irradiation results. However, the problem is that many obscure points still remain about the basic physics of single SIA and SIA loops in Fe. SIA and SIA loop migration mechanisms are especially still being debated.

Indeed, according to MD simulations with empirical interatomic potentials, two regimes of single SIA migration can be broadly identified (see e.g. [57]). At low temperature (say, well below 600 K), the diffusion mechanism is fairly complicated: the SIA spends a significant time in a $\langle 1\,1\,0\rangle$ dumbbell configuration, followed by a series of fast jumps in one direction, via the $\langle 1\,1\,1\rangle$ crowdion mechanism. The change of $\langle 1\,1\,1\rangle$ migration direction takes place generally during the time spent as $\langle 1\,1\,0\rangle$ dumbbell. At high temperature (above 600 K) both the time spent in the $\langle 1\,1\,0\rangle$ configuration and the length of the $\langle 1\,1\,1\rangle$ macrojumps decrease, thereby approaching a full 3D migration regime. These simulations provide an effective migration energy for the single SIA between 0.04 and 0.08 eV, depending on the interatomic potential used [57]. If the two temperature regimes are distinguished, a higher migration energy (close to 0.1 eV) is found at high temperature, while at low temperature the effective migration energy remains extremely low (0.04 eV or even less) [21,57]. The energy for change of $\langle 1\,1\,1\rangle$ direction is found to be 0.1–0.3 eV [22,58,59,73]. Yet, while the actual SIA diffusion mechanisms change with temperature and changes of $\langle 1\,1\,1\rangle$ migration direction become more frequent with temperature rise, the effective migration energy remains lower than the rotation energy.

This picture contrasts with the experimental data on SIA migration in Fe, which suggest a migration (and rotation) energy of 0.3 eV (e.g. [70] and references therein). In addition, recent ab initio calculations show that the rotation energy from the $\langle 1\,1\,0\rangle$ to the $\langle 1\,1\,1\rangle$ SIA configuration may be higher than 0.7 eV [63] (to be compared to the about 0.1 eV currently predicted by empirical many-body potentials [73,74]). In these conditions, the rotation from $\langle 1\,1\,0\rangle$ to $\langle 1\,1\,1\rangle$ which, according to MD simulations with current empirical potentials, governs the migration mechanism of SIA in Fe, would become highly unlikely. The migration mechanism would then be closer to the one proposed already 40 years ago by Johnson [98], involving both rotation (change of $\langle 1\,1\,0\rangle$ direction) and migration (jump to first nearest neighbour), keeping the $\langle 1\,1\,0\rangle$ dumbbell configuration. The migration energy for this mechanism was computed by Johnson to be 0.3 eV and the same value has been computed recently using first principle calculations

[99]. If this mechanism was the correct one, then, most likely, also at low temperature the single SIA would migrate along a fully 3D path, although no simulation studies of this type, with potentials predicting a high energy difference between the ⟨1 1 0⟩ and ⟨1 1 1⟩ configurations, currently exist. A more stable ⟨1 1 0⟩ dumbbell may also partially change the description of the motion of small SIA clusters, predicting higher effective migration energies, and shifting the size above which the collection of ⟨1 1 1⟩ crowdions is energetically preferred to the collection of ⟨1 1 0⟩ dumbbells.

These issues are presently being debated, new empirical many-body potentials, yielding higher energy difference between the ⟨1 1 0⟩ and ⟨1 1 1⟩ interstitial configurations are being proposed [100] and it is expected that soon the current ideas concerning the mechanism of SIA migration in Fe will have to be revised. In this framework, in the current model it was deliberately decided to use the simplest possible SIA and SIA cluster description, based on existing examples from Refs. [21–25]. This corresponds to assuming full 3D motion for the single SIA and essentially unidimensional motion for SIA clusters, with migration energy equal to ~0.04 eV and prefactor decreasing with size. The only alternative choice could be to use 0.3 eV as migration energy for the single SIA. Still, considering the strong tendency of SIA to cluster and their anyhow fast motion, this is not expected to have a major impact on the results.

Another weakness of the model is that, at present, it does not differentiate between glissile 1/2⟨1 1 1⟩ and sessile ⟨1 0 0⟩ loops. It simply treats SIA clusters of different sizes with different ⟨1 1 1⟩ glide directions. In addition, the strain field associated to loops is considered isotropic and spherical. The effect of transformation to sessile ⟨1 0 0⟩ loops, whatever the mechanism leading to this transformation should be [101,102], is implicitly introduced in the form of 'generic traps'. In general, generic traps substitute for unknown, or non-allowed-for, mechanisms of interaction of SIA (clusters particularly) with each other and with other defects (for instance elastic interactions [37,104] and effective trapping at vacancies [103] or between repulsive impurities [86]) or with sinks (dislocations), which globally are expected to decrease the mobility of these objects. This method, while not fully satisfactory from the strictly physical viewpoint, seems however rather appropriate until more complete understanding of the mechanisms of transformation of glissile SIA clusters into sessile loops and interaction with each other and with other defects become available. For instance, the introduction of the SIA loop strain field calculated from the elasticity theory in a KMC model is feasible [37,104] and, most likely, more appropriate than assuming a spherical strain field, as done in this work. Yet, in a recent MD study [105] it was concluded that clusters up to about 2 nm in diameter cannot be described as dislocation loops in the isotropic continuum approach. Thus, before going into such refinements, a clearer and more complete description of SIA and SIA cluster properties in Fe is necessary. In addition, it should be born in mind that, the more precise the description of the physics involved, the longer the computing time and the smaller the accessible time- and space-scales. The objective should be the selection of only the key phenomena responsible for damage evolution, in a trade-off between reliability and computational efficiency, following a systematic, step-by-step validation approach.

Having said that, improvements to the model should be introduced and are envisaged. Broadly, these improvements should correspond to making explicit those effects that are now implicitly hidden in the 'generic traps'.

To start with, the model already includes some features that should make the simulation more realistic, but were not used in this work. The capture volume of large SIA loops can be described as an annulus of radius $r_{\alpha,1}$ around the dislocation line, rather than as a sphere. In addition, dislocations can be introduced as segments, acting as linear sinks. These options will be tested in the future, to assess up to what extent they improve the agreement with experiments.

Other mechanisms to be introduced and tested, aimed at better describing SIA and SIA loops, are, for instance: the repulsion between Cu precipitates [78] and or (mobile) interstitial impurity atoms (C, N [86]) and SIA or SIA loops; the trapping of SIA loops due to single vacancies before annihilation [103]; and a better description of the interaction between SIA loop strain fields, e.g. using the elastic theory [37,104], or other adequate approximations. It remains to be demonstrated whether these mechanisms will be enough to completely replace the current 'generic traps' and provide better agreement with experiments. If so, the traditionally assumed SIA loop formation mechanism, based on the idea of trapping of SIA at C and N impurities as centres of nucleation, may become questionable and the ab initio indication of weak interaction of SIA with these impurities [86] supported. If, on the other hand, generic traps are still necessary, it will mean that the picture is not complete and some mechanisms remain unknown.

A more precise treatment of the binding energies of vacancy clusters and Cu-vacancy complexes, based on atomic-level studies [87,88], should be also introduced, in order to better reproduce single vacancy, vacancy-Cu pair or Cu atom emission from clusters. This upgrade is indeed already underway [89]. Currently, the model does not allow the emission of a single Cu atom from a mixed cluster, but it is plausible that a mobile mixed cluster may drop a Cu atom and leave it in its trail. In addition, the trapping of vacancies at mobile

traps, explicitly associated to C or N atoms [86], or solute atoms other than Cu, should be considered.

Finally, more refined treatments of the incoming particle damage are also envisaged. For instance, a more precise simulation of very high energy electrons could be to introduce point defects as a distribution of very low energy cascades. In this case, a method similar to the ion irradiation described in Section 2.1.2 could be adopted. For neutrons, a possible improvement could be to group all subcascades corresponding to the same, larger cascade, according to the INCAS decomposition, in the same region of the simulation box, so as to take into account the possibly higher local recombination rate, due to intra-subcascade interaction.

5. Conclusions

We have developed an object KMC code which allows the simulation, within acceptable approximations, of individual cascade ageing as well as neutron, ion or electron irradiation processes in Fe and Fe–Cu alloys. In this article we have described in detail the model and presented a first set of studies aiming at establishing an appropriate set of parameters, within commonly accepted assumptions and approximations. The approach we followed is based on the adoption of mechanisms and parameters coming mostly from atomistic simulations, sensitivity studies of the effect of changing parameters in simple cascade ageing simulations, comparison with other models and, finally, tuning on experimental results. The objective, is to find a trade-off between physical reliability and computing time.

This simple model, based sometimes on rough assumptions, such as spherical interaction volumes (even in the case of SIA and SIA clusters), succeeds, as shown, in satisfactorily reproducing experimental results of Fe alloy irradiation under different conditions. However, 'generic traps' for interstitials must be introduced in order to have good agreement with the experiments. The assumption that only single point-defects are mobile, which may be an indirect way of introducing traps, aside from contrasting with the commonly accepted fact that point-defect clusters do move, can produce reasonable results in the case of electron irradiation, but proves inadequate under cascade damage conditions. The choice of the capture radius, surprisingly, does not play a major role.

These promising results make us believe that a step-by-step approach, introducing new mechanisms in the OKMC model and assessing their effect, in interplay between simulation results and modelling-oriented experiments, covering different conditions, will not only lead to the elaboration of an optimised parameter set, but will also, eventually, help identify the nature of some, still elusive, features produced during irradiation in metals.

Acknowledgments

The authors wish to acknowledge very fruitful discussions with M. Hou (ULB) and A. Legris (USTL), as well as the contribution of A. Barbu (CEA). This work was performed in the framework of the international REVE initiative, which aims at producing a multiscale suite of integrated codes capable of simulating radiation effects in structural nuclear materials for industrial applications. This work is part of the European PERFECT project, starting in 2004 and supported by the European Commission (FI6O-CT-2003-508840).

Appendix A. Computational details

The parameters for the description of the behaviour of the different objects treated by the LAKIMOCA package are read by the code from different input text files containing, for each object, as a function of size, the capture radii, attempt frequencies, activation energies, binding energies, etc. These files can be created by a short pre-processing code, by which it is easy to change at will the parameterisation and create different possible combinations, to be tested in parallel for sensitivity studies.

No satisfactory scheme to parallelise an OKMC code has yet been found. Nonetheless, the LAKIMOCA package has been optimised to be as fast possible, despite being a serial code. In particular, an important improvement has been achieved by an adaptation of the link cell method used in MD to build the neighbour list, at least for objects below a certain size. In this case, the recombination radii play the role of the interatomic potential range in MD. Only for objects larger than a given size there is no neighbour list treatment and the possible interaction with all objects in the box has to be checked. The simulation time depends not only on type of impinging particles, dose, dose-rate and temperature, but also on box-size, parameter set and detailed features of the model. The irradiation conditions of RPV steels in operation represent an extreme case, but are satisfactorily handled by the code. To give an idea of the performance, our code can simulate 30 years of irradiation under RPV conditions ($\sim$0.1 dpa/$(3600 \times 24 \times 365 \times 30)$ s $\sim 10^{-11}$ dpa/s, $\sim$300 °C), using set B with traps, in a $100a_0 \times 100a_0 \times 100a_0$ box, in a couple of days of CPU time. The computational time, on a Pentium 4 processor, for some of the simulations conducted for the present work are reported in Table 6. The CPU consumption is proportional to the number

Table 6
Characteristic computing time on a Pentium IV based PC

Simulation type	Characteristics: box size in bcc lattice unit cell	CPU time (s)
Single cascade annealing	$100 \times 100 \times 100$	$\approx$1 s
Thin foil electron irradiation (1.5×10^{-4} $e^-/cm^3/s$) 100 °C–1200 s	$100 \times 100 \times 1000$	$\approx$1 day
Bulk HFIR (10^{-6} dpa/s) 70 °C–0.1 dpa	$200 \times 200 \times 200$	$\approx$1 day
Bulk HFIR/10^5 (10^{-11} dpa/s)–300 °C–0.1 dpa–0.2%Cu	$100 \times 100 \times 100$	$\approx$2 days

of jumps to be processed per simulated unit time, Δt; thus the lower the temperature, the smaller the necessary amount of computation. The single SIA jump, which is the most frequent event, is the limiting factor. The larger the number of vacancies (isolated or in cluster) and SIA clusters, the faster the annihilation of the moving interstitials and the lower the CPU time.

The output of the package provides directly the cluster size distribution, either at each decade or every fixed amount of timesteps, for every possible complex object (SIA clusters, vacancy clusters, vacancy-copper complexes,...), as well as other pieces of information, such as the total number of defects, the number of defects leaving the box, and so on. The statistical treatment of the output is done using post-processing programs.

References

[1] G.R. Odette, B.D. Wirth, J. Nucl. Mater. 251 (1997) 157.
[2] W.J. Phythian, C.A. English, J. Nucl. Mater. 205 (1993) 162.
[3] C.A. English, J.M. Hyde, S.R. Ortner, in: S. Ishino, B.L. Eyre, I. Kimura (Eds.), Proceedings of International Symposium on Mechanisms of Material Degradation and Non-Destructive Evaluation in Light Water Reactors, Osaka, Japan, 27–29 May 2002, Institute of Nuclear Safety, Inc., Japan, 2002.
[4] G.R. Odette, C.L. Liu, B.D. Wirth, Mater. Res. Soc. Symp. Proc. 439 (1997) 457.
[5] P. Auger, P. Pareige, S. Welzel, J-C. van Duysen, J. Nucl. Mater. 280 (2000) 331.
[6] M.K. Miller, B.D. Wirth, G.R. Odette, Mater. Sci. Eng. A 353 (2003) 133.
[7] R.S. Averback, T. Diaz de la Rubia, Solid State Phys. 51 (1998) 281.
[8] J.A. Brinkman, J. Appl. Phys. 25 (8) (1954) 961.
[9] A. Seeger, in: Proceedings of 2nd UN Conference on Peaceful Uses of Atomic Energy, IAEA, 1958, p. 250.
[10] J.B. Gibson, A.N. Goland, M. Milgram, G.H. Vineyard, Phys. Rev. 120 (4) (1960) 1229.
[11] C. Erginsoy, G.H. Vineyard, A. Englert, Phys. Rev. 133-2A (1964) A595.
[12] M.W. Guinan, J.H. Kinney, J. Nucl. Mater. 103&104 (1981) 1319.
[13] D.J. Bacon, A.F. Calder, J.M. Harder, S.J. Wooding, J. Nucl. Mater. 205 (1993) 52.
[14] M. Spaczér, A. Caro, M. Victoria, T. Diaz de la Rubia, J. Nucl. Mater. 212–215 (1994) 164.
[15] W.J. Phythian, R.E. Stoller, A.J.E. Foreman, A.F. Calder, D.J. Bacon, J. Nucl. Mater. 223 (1995) 245.
[16] J.M. Delaye, D. Ghaleb, J. Nucl. Mater. 244 (1997) 22.
[17] R.E. Stoller, J. Nucl. Mater. 276 (2000) 22.
[18] D.J. Bacon, F. Gao, Yu.N. Osetsky, J. Nucl. Mater. 276 (2000) 1.
[19] C.S. Becquart, C. Domain, A. Legris, J-C. van Duysen, J. Nucl. Mater. 280 (2000) 73.
[20] C.S. Becquart, C. Domain, J-C. van Duysen, J.M. Raulot, J. Nucl. Mater. 294 (2001) 274.
[21] N. Soneda, T. Diaz de la Rubia, Philos. Mag. A 78 (1998) 995.
[22] F. Gao, D.J. Bacon, A.V. Barashev, H.L. Heinisch, Mater. Res. Soc. Symp. Proc. 540 (1999) 703.
[23] M.J. Caturla, N. Soneda, E. Alonso, B.D. Wirth, T. Díaz de la Rubia, J.M. Perlado, J. Nucl. Mater. 276 (2000) 13.
[24] J. Marian, B.D. Wirth, J.M. Perlado, T. Díaz de la Rubia, R. Schäublin, D. Lodi, M. Hernández, G. de Diego, D.G. Briceño, R.E. Stoller, Mater. Res. Soc. Symp. Proc. 650 (2001) R3.2.1-6.
[25] N. Soneda, S. Ishino, A. Takahashi, K. Dohi, J. Nucl. Mater. 323 (2003) 169.
[26] C. Domain, C.S. Becquart, J.-C. van Duysen, Mater. Res. Soc. Symp. Proc. 540 (1999) 643.
[27] C. Domain, C.S. Becquart, J.-C. van Duysen, Mater. Res. Soc. Symp. Proc. 650 (2001) R3.25.1-6.
[28] L. Malerba, C.S. Becquart, M. Hou, C. Domain, in: Proceedings of International Symposium on Microstructural Processes in Irradiated Materials, TMS Annual Meeting, San Diego, 3–6 March 2003, Philos. Mag., in press.
[29] F. Maurice, N.V. Doan, Simulation de l'évolution de populations de défauts dans un cristal par la méthode de Monte Carlo, Rapport CEA-R-5101 (1981).
[30] K. Morishita, R. Sugano, B.D. Wirth, J. Nucl. Mater. 323 (2003) 243.
[31] W.M. Young, E.W. Elcock, Proc. Phys. Soc. 89 (1966) 735.
[32] L.R. Greenwood, R.K. Smither, SPECTER: Neutron Damage Calculations for Materials Irradiations, ANL/FPP-TM-197 Report, Argonne NL, January 1985; code available at: http://www.nea.fr/abs/html/psr-0263.html; see also L.R. Greenwood, J. Nucl. Mater. 216 (1994) 29.
[33] S. Jumel, J.-C. van Duysen, J. Nucl. Mater. 328 (2004) 151.
[34] M.J. Norgett, M.T. Robinson, I.M. Torrens, Nucl. Eng. Des. 33 (1975) 50.
[35] ASTM E693, Annual Book of ASTM Standards, 12.02 (1994).
[36] B.M. Athenes, P. Bellon, G. Martin, Philos. Mag. A 76 (1997) 565.

[37] N.M. Ghoniem, S.H. Tong, J. Huang, B.N. Singh, M. Wen, J. Nucl. Mater. 307–311 (2002) 843.
[38] B. Bortz, M.H. Kalos, J.L. Lebowitz, J. Comp. Phys. 17 (1) (1975) 10.
[39] H.L. Heinisch, B.N. Singh, J. Nucl. Mater. 307–311 (2002) 876.
[40] I.M. Robertson, M.A. Kirk, W.E. King, Scr. Mater. 18 (1984) 317.
[41] Y. Shimomura, H. Fukushima, M.W. Guinan, J. Nucl. Mater. 174 (1990) 210.
[42] L.L. Horton, J. Bentley, K. Farrell, J. Nucl. Mater. 108&109 (1982) 222.
[43] A. Hardouin Duparc, C. Moingeon, N. Smetniansky-de-Grande, A. Barbu, J. Nucl. Mater. 302 (2002) 143.
[44] M.L. Jenkins, C.A. English, B.L. Eyre, Philos. Mag. A 38 (1978) 97.
[45] A.C. Nicol, M.L. Jenkins, M.A. Kirk, Mater. Res. Soc. Symp. Proc. 650 (2001) R1.3.1-6.
[46] M. Victoria, N. Baluc, C. Bailat, Y. Dai, M.I. Luppo, R. Schäublin, B.N. Singh, J. Nucl. Mater. 276 (2000) 114.
[47] A. Hempel, M. Saneyasu, Z. Tang, M. Hasegawa, G. Brauer, F. Plazaola, S. Yamaguchi, F. Kano, A. Kawai, in: M.L. Hamilton, A.S. Kumar S.T. Rosinski, M.L. Grossbeck (Eds.), Effects of Radiation on Materials: 19th International symposium, ASTM STP 1366, ASTM, West Conshohocken, PA, 2000, p. 560.
[48] Y. Nagai, Z. Tang, M. Hasegawa, T. Kanai, M. Saneyasu, Phys. Rev. B 63 (2001) 134110.
[49] M. Eldrup, B.N. Singh, S.J. Zinkle, T.S. Byun, K. Farrell, J. Nucl. Mater. 307–311 (2002) 912.
[50] M. Eldrup, B.N. Singh, J. Nucl. Mater. 323 (2003) 346.
[51] F. Maury, N. Lorenzelli, M.H. Mathon, C.H. de Novion, P. Lagarde, J. Phys.: Condens. Mater. 6 (1994) 569.
[52] P. Auger, P. Pareige, S. Welzel, J-C. Van Duysen, J. Nucl. Mater. 280 (2000) 331.
[53] N. Lê, A. Barbu, D. Liu, F. Maury, Scr. Metall. Mater. 26 (1992) 771.
[54] W.J. Phythian, A.J.E. Foreman, C.A. English, J.T. Buswell, M. Hetherington, K. Roberts, S. Pizzini, in: R.E. Stoller, A.S. Kumar, D.S. Gelles (Eds.), Effects of Radiation on Materials: 15th International Symposium, ASTM STP 1125, ASTM, Philadelphia, 1992, p. 131.
[55] K. Fukuya, K. Ohno, H. Nakata, S. Dumbill, J.M. Hyde, J. Nucl. Mater. 312 (2003) 163.
[56] Yu.N. Osetsky, D.J. Bacon, A. Serra, B.N. Singh, S.I. Golubov, J. Nucl. Mater. 276 (2000) 65.
[57] Yu.N. Osetsky, Defect Diffusion Forum 188–190 (2001) 71.
[58] B.D. Wirth, G.R. Odette, D. Maroudas, G.E. Lucas, J. Nucl. Mater. 244 (1997) 185.
[59] Yu.N. Osetsky, M. Victoria, A. Serra, S.I. Golubov, V. Priego, J. Nucl. Mater. 251 (1997) 34.
[60] N. Soneda, T. Díaz de la Rubia, Philos. Mag. A 81 (2001) 331.
[61] A.D. Brailsford, R. Bullough, J. Nucl. Mater. 44 (1972) 121.
[62] A. Barbu, C.S. Becquart, J.-L. Bocquet, J. Dalla Torre, C. Domain, in: Proceedings of International Symposium on Microstructural Processes in Irradiated Materials, TMS Annual Meeting, San Diego, 3–6 March 2003, Philos. Mag., in press.
[63] C. Domain, C.S. Becquart, Phys. Rev. B 65 (2001) 024103/1-14.
[64] C.S. Becquart, C. Domain, Nucl. Instrum. and Meth. B 202 (2003) 44.
[65] J. Dural, J. Ardonceau, J.C. Roussett, Le Journal de Physique 38 (1977) 1007.
[66] M. Biget, R. Rizk, P. Vajda, A. Bessis, Solid State Commun. 16 (1975) 949.
[67] R.E Stoller, in: A.S. Kumar, D.S. Gelles, R.K. Nanstad, E.A. Little (Eds.), Effects of Radiation on Materials: 16th International symposyum, ASTM STP 1175, ASTM, Philadelphia, 1993, p. 394.
[68] A. Souidi, M. Hou, C.S. Becquart, C. Domain, J. Nucl. Mater. 295 (2001) 179.
[69] B. Grant, J.M. Harder, D.J. Bacon, J. Nucl. Mater. 171 (1990) 412.
[70] S. Takaki, J. Fuss, H. Kugler, U. Dedek, H. Schultz, Radiat. Eff. 79 (1983) 87.
[71] W. Chambron, J. Verdone, P. Moser, in: Conference on Fundamental Aspects of Radiation Damage in Metals, Gatlinburg, 1975, p. 26.
[72] H. Maeta, F. Ono, T.J. Kittaka, J. Phys. Soc. Jpn. 53 (1984) 4353.
[73] F. Gao, G. Henkelman, W.J. Weber, L.R.L. Corrales, H. Jónsson, Nucl. Instrum. and Meth. B 202 (2003) 1.
[74] R.C. Pasianot, A.M. Monti, G. Simonelli, E.J. Savino, J. Nucl. Mater. 276 (2000) 230.
[75] F. Maury, A. Lucasson, P. Lucasson, P. Moser, F. Faudot, J. Phys.: Condens. Matter 2 (1990) 9291.
[76] Vienna Ab Initio Package: G. Kresse, J. Hafner, Phys. Rev. B 47 (1993) 558;
Phys. Rev. B 49 1994 14251.
[77] J. Marian, B.D. Wirth, J.M. Perlado, G.R. Odette, T. Díaz de la Rubia, Phys. Rev. B 64 (2001) 144102/1-11;
J. Marian, B.D. Wirth, A. Caro, B. Sadigh, G.R. Odette, J.M. Perlado, T. Díaz de la Rubia, Phys. Rev. B 65 (2002) 094303/1-5.
[78] D. Lodi, L. Malerba, C. Domain, unpublished.
[79] A. Vehanen, P. Hautojärvi, J. Johansson, J. Yli-Kauppila, P. Moser, Phys. Rev. B 25 (1982) 762.
[80] J.R. Beeler Jr., R.A. Johnson, Phys. Rev. 156 (1967) 677.
[81] G. Brauer, K. Popp, Phys. Status Solidi 102 (1987) 79.
[82] A. Möslang, E. Albert, E. Recknagel, A. Weidinger, P. Moser, Hyperfine Interactions 15 (1983) 409.
[83] H.E. Schaefer, K. Maier, M. Weller, D. Herlach, A. Seeger, J. Diehl, Scr. Metall. 11 (1977) 803.
[84] A. Hardouin du parc, PhD Thesis, Paris XI-Orsay University (1997), ISSN 0429-3460, CEA report R-5791.
[85] C. Domain, C.S. Becquart, in: Proceedings of International Symposium on Microstructural Processes in Irradiated Materials, TMS Annual Meeting, San Diego, 3–6 March 2003, Philos. Mag., in press.
[86] C. Domain, C.S. Becquart, J. Foct, Phys. Rev. B 69 (2004) 144112.
[87] A. Takahashi, N. Soneda, S. Ishino, G. Yagawa, Phys. Rev. B 67 (2003) 24104-1/9.
[88] D. Kulikov, L. Malerba, M. Hou, SCK•CEN Report BLG-956, April 2004.
[89] L. Malerba, C. Domain, C.S. Becquart, D. Kulikov, COSIRES 2004, in preparation.

[90] W. Schilling, J. Nucl. Mater. 69&70 (1978) 465.
[91] M.T. Robinson, Phys. Rev. B 40 (1989) 10717.
[92] M. Hou, Phys. Rev. B 31 (1985) 4178.
[93] C.S. Becquart, C. Domain, L. Malerba, M. Hou, COSIRES 2004, in preparation.
[94] L.E. Rehn, R.C. Birtcher, J. Nucl. Mater. 205 (1993) 31.
[95] S.J. Zinkle, B.N. Singh, J. Nucl. Mater. 199 (1993) 173.
[96] C.A. English, W.J. Phythian, J.T. Buswell, J.R. Hawthorne, P.H. Ray, in: R.E. Stoller, A.S. Kumar, D.S. Gelles (Eds.), Effects of radiation on materials: 15th International Symposium, ASTM STP 1125, Philadelphia, 1992, p. 93.
[97] M.G. Burke, M.K. Miller, Journal de Physique, Colloque C6, Supplément au no. 11, 49 (1988) C6-283-C6-288.
[98] R.A. Johnson, Phys. Rev. 134 (1964) A1329.
[99] C.-C. Fu, F. Willaime, CEA Annual Report 2003, DMN/SRMP/NT/2003-06, p. 52.
[100] M.I. Mendelev, S. Han, D.J. Srolovitz, G.J. Ackland, D.Y. Sun, M. Asta, Philos. Mag. 83 (2003) 3977.
[101] B.L. Eyre, R. Bullough, Philos. Mag. 12 (1965) 31.
[102] J. Marian, B.D. Wirth, J.M. Perlado, Phys. Rev. Lett. 88 (2002) 255507.
[103] M.A. Puigvi, A. Serra, N. de Diego, Yu.N. Osetstky, D.J. Bacon, Philos. Mag. Lett. 84 (2004) 257.
[104] T. Hudson, M.J. Caturla, S.L. Dudarev, A.P. Sutton, in: Proceedings of International Symposium on Microstructural Processes in Irradiated Materials, TMS Annual Meeting, San Diego, 3–6 March 2003, Philos. Mag., submitted for publication.
[105] M.A. Puigvi, Yu.N. Osetsky, A. Serra, Philos. Mag. 83 (2003) 857.